REVISITING DEEP ENSEMBLE FOR OUT-OF-DISTRIBUTION DETECTION: A LOSS LANDSCAPE PERSPECTIVE

Kun Fang[1], Qinghua Tao[2], Xiaolin Huang[1] and Jie Yang[1]

[1]Department of Automation, Shanghai Jiao Tong University, {fanghenshao,xiaolinhuang,jieyang}@sjtu.edu.cn
[2]ESAT-STADIUS, KU Leuven, Belgium, qinghua.tao@esat.kuleuven.be

ABSTRACT

Existing Out-of-Distribution (OoD) detection methods address to detect OoD samples from In-Distribution (InD) data mainly by exploring differences in features, logits and gradients in Deep Neural Networks (DNNs). We in this work propose a new perspective upon *loss landscape* and *mode ensemble* to investigate OoD detection. In the optimization of DNNs, there exist many local optima in the parameter space, or namely *modes*. Interestingly, we observe that these independent modes, which all reach low-loss regions with InD data (training and test data), yet yield significantly different loss landscapes with OoD data. Such an observation provides a novel view to investigate the OoD detection from the loss landscape, and further suggests significantly fluctuating OoD detection performance across these modes. For instance, FPR values of the RankFeat [1] method can range from 46.58% to 84.70% among 5 modes, showing uncertain detection performance evaluations across independent modes. Motivated by such diversities on OoD loss landscape across modes, we revisit the deep ensemble method for OoD detection through mode ensemble, leading to improved performance and benefiting the OoD detector with reduced variances. Extensive experiments covering varied OoD detectors and network structures illustrate high variances across modes and validate the superiority of mode ensemble in boosting OoD detection. We hope this work could attract attention in the view of independent modes in the loss landscape of OoD data and more reliable evaluations on OoD detectors.

Keywords Out-of-distribution detection · Loss landscape · Mode · Ensemble

1 Introduction

For years Deep Neural Networks (DNNs) have shown powerful abilities in fitting In-Distribution (InD) data. Given a DNN f well-trained on data from some distribution $\mathcal{P}_{in}$, f also performs well on the test data, which is commonly regarded as being from the same distribution $\mathcal{P}_{in}$ as the training data [2]. However, the generalization ability of f on the data from an out distribution $\mathcal{P}_{out}$ is still prohibitive, which brings a large number of researches [3, 4, 5, 6, 7, 8, 9, 1, 10, 11, 12, 13] trying to detect Out-of-Distribution (OoD) samples in the inference stage, known as the popular OoD detection problem [14, 15].

In the existing works for OoD detection, the key is to find the different responses from DNNs towards InD and OoD data and then to leverage such differences to distinguish OoD samples. There are various ways to measure such differences with DNNs, such as the logits or probabilities [3, 4, 6, 12], the features or activations [5, 8, 1, 10, 11, 12, 13], the parameter gradients [7, 9], etc. For example, an early work MSP [3] directly uses the maximum softmax probability to measure the abnormal predictive confidence from DNNs on OoD data. GradNorm [9], as its name suggests, uses the norm of the gradients as the detection metric, since the gradients of InD and OoD data are distinctively different *w.r.t* the carefully-designed loss in the paper. A recent work RankFeat [1] proposes to remove the rank-1 feature matrix in the forward propagation during inference, as the rank-1 matrix is the mostly likely to contain information causing the over-confidence of OoD predictions.

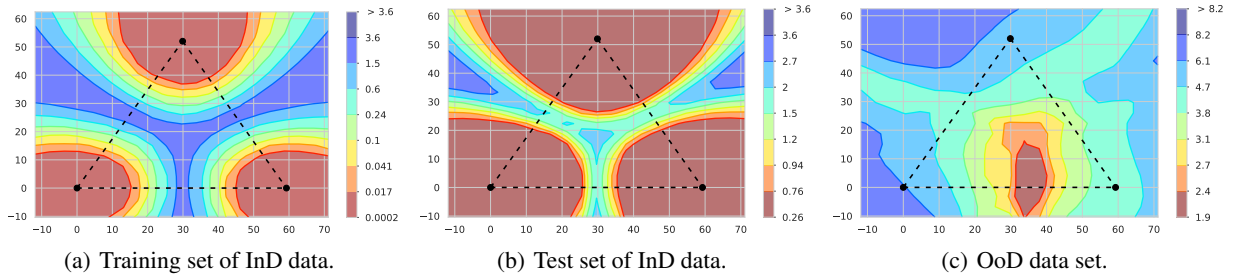| (a) Training set of InD data. | (b) Test set of InD data. | (c) OoD data set. |

Figure 1: An illustration on the loss landscape of InD and OoD data, as a function of network weights in a two-dimensional subspace. The 3 isolated modes are located in similar low loss regions on the InD data, but in significantly different loss areas for the OoD data. The visualization technique follows [16]. Refer to Fig.4 for more details on each mode.

In this work, we address the OoD detection problem from a novel perspective: *loss landscape* and *mode ensemble*. The loss landscape of DNNs is extremely complex and highly non-convex due to the millions of parameters and non-linear activations, which inevitably results in numerous isolated optima (*modes*) in the loss landscape, suggested by lots of pioneering works [17, 16, 18, 19]. Nevertheless, these works all focus on mode properties in the loss landscape of InD data. By introducing the loss landscape of OoD data and visualizing locations of 3 isolated modes in Fig.1 and Fig.4, we observe a key phenomenon on those isolated modes that are trained independently on InD data *w.r.t* different random seeds: These modes, even though located in isolation in the loss landscape, undoubtedly all reach low-loss regions on the InD data, shown in Fig.1(a) and Fig.1(b), yet, their locations in the loss landscape for the OoD data instead hold strong diversities, *i.e.*, these modes show significantly distinct loss regions for the OoD data, shown in Fig.1(c) and Fig.4 with more details.

Considering such diversities of these modes in the OoD loss landscape, there naturally exists a hypothesis that these independent modes, though all with consistently good performance on InD data, might hold a large variance on the OoD detection results even under the same OoD detector. For example, in Fig.2, the RankFeat method [1] achieves fluctuating FPR values ranging from 46.58% to 84.70% among isolated modes of the same network structure on the same OoD data set. Besides, detection results between 2 OoD detectors could be opposite on isolated modes, *e.g.*, RankFeat outperforms Energy [6] on mode-3 but falls inferior on mode-1 and mode-2. Such high detection variances among independent modes have been ignored by the research community and bring difficulties in developing and evaluating OoD detectors. All these findings hence motivate us to explore OoD detection across independent modes, rather than within a single mode, to leverage the diversities reflected on the loss landscape of OoD data.

Accordingly, we revisit the deep ensemble method [20] to perform mode ensemble for OoD detection, which is shown to bring substantial variance reduction and performance improvements, and helps the evaluation on OoD detectors. Specifically, for different types of OoD detectors, we design corresponding mode ensemble strategies by ensembling the output logits or features from multiple isolated modes, then the ensembled outputs are exploited by those OoD detectors. Besides, a theoretical derivation is provided to show the superiority of ensembling modes over the average of single modes. Our experiments for mode ensemble are extensive and comprehensive: (i) Various state-of-the-art (SOTA) OoD detection methods are involved, including logits-, features- and gradients-based detectors; (ii) Small-scale, large-scale data sets and distinct network structures, such as the prevailing Vision Transformer (ViT, [21]), are covered. All these theoretical and empirical results support our viewpoint: there exist high variances in OoD detection performance of independent modes, and mode ensemble could bring substantial performance improvements and help the evaluation of OoD detectors, which we hope could benefit the research community with the perspective of independent modes in the loss landscape of OoD data.

Our contributions are summarized as follows:

- We propose a novel perspective, *loss landscape* and *mode ensemble*, to analyze and address the OoD detection problem. Our observation shows that isolated modes hold diversified loss landscapes on OoD data, resulting in high variances of OoD detection results among these modes.

- We revisit the deep ensemble method to perform mode ensemble, design corresponding ensemble strategies for different types of OoD detectors, and find more stable and better OoD detection results.

- Extensive and comprehensive empirical results including ablation studies and comparisons with other ensemble methods have verified the uncertainties of single modes and advantages of mode ensemble in the OoD detection task.
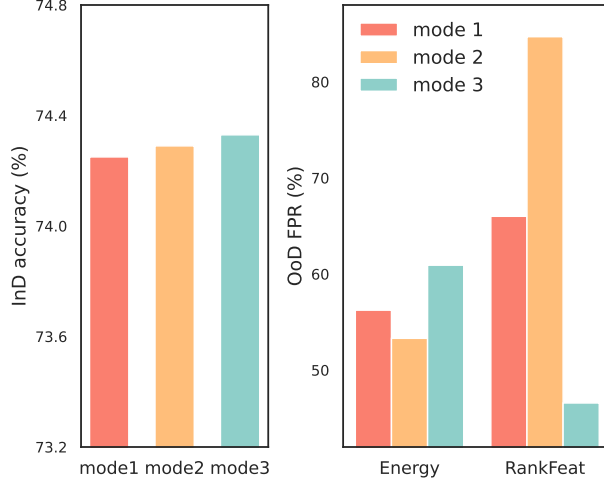
Figure 2: There exists a high variance among the OoD detection results (FPR95) of 3 independent modes on 2 OoD detectors Energy [6] and RankFeat [1] (the right panel), while the 3 modes all hold good and similar recognition accuracy on the InD test set (the left panel).

In the following, Sec.2 elaborates our mode ensemble for OoD detection. Experiments are presented in Sec.3 and related works are shown in Sec.4. Section 5 draws conclusions and discussions.

2 OoD detection with ensemble modes

In this section, we firstly outline the background of OoD detection in Sec.2.1, then give detailed elaboration on the loss landscape and mode ensemble of our method in Sec.2.2, and provide theoretical analyses in Sec.2.3.

2.1 Preliminary: OoD detection

Given a neural network $f : \mathbb{R}^D \to \mathbb{R}^C$, its training data is from some distribution $\mathcal{P}_{\mathrm{in}}$, known as the in distribution. Once deployed, f will encounter unseen data that could be from either the known distribution $\mathcal{P}_{\mathrm{in}}$ or an unknown out distribution $\mathcal{P}_{\mathrm{out}}$. OoD detection aims at deciding whether one new sample $\boldsymbol{x} \in \mathbb{R}^D$ is from $\mathcal{P}_{\mathrm{in}}$ or $\mathcal{P}_{\mathrm{out}}$.

Generally, OoD detection is formulated as a binary classification problem with a decision function $D(\cdot)$ and a scoring function $S(\cdot)$:

$$D(\boldsymbol{x}) = \left\{ \begin{array}{ll} \mathrm{InD}, & S(\boldsymbol{x}) > \lambda, \\ \mathrm{OoD}, & S(\boldsymbol{x}) < \lambda. \end{array} \right. \tag{1}$$

The scoring function $S(\cdot)$ assigns a score $S(\boldsymbol{x})$ for a new sample $\boldsymbol{x}$. If the score $S(\boldsymbol{x})$ is greater than a threshold λ, then $\boldsymbol{x}$ will be viewed as an InD sample by the decision function $D(\cdot)$, and vice versa. λ is appropriately chosen so that a large proportion (*e.g.*, 95%) of InD data will be correctly classified. A justified scoring function $S(\cdot)$ is the key to successfully distinguish OoD data from InD data.

2.2 Mode ensemble for OoD detection

2.2.1 Loss landscape

Inspired by prior works investigating the loss landscape and mode connectivity for the generalization ability of DNNs on the InD test data [17, 16, 18, 19], we propose to analyze the OoD detection problem from the loss landscape perspective. Specifically, our analysis focuses on those *independent* or *isolated* modes that are obtained by training multiple DNNs merely on the InD data *w.r.t* different random seeds. As the random seed dominates the initialization of DNNs and the noise in the SGD optimization, these modes are actually in correspondence to unique training trajectories, and thus are independent and isolated. Fig.3 illustrates 3 distinct training trajectories of 3 modes *w.r.t* 3 different random seeds by visualizing features learned by the checkpoints during training.
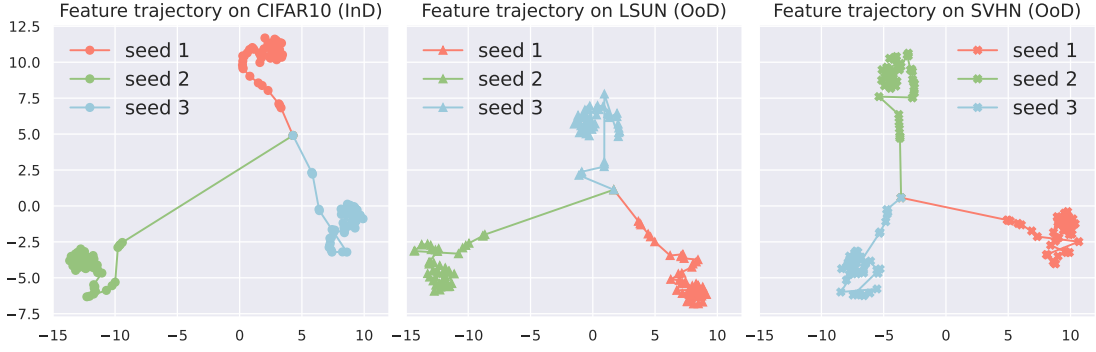
3

Figure 3: An illustration on the feature trajectories during model training on CIFAR10 (InD) *w.r.t* 3 random seeds. 48 checkpoints in each training are sampled. The learned features of CIFAR10 (left), LSUN (OoD, middle) and SVHN (OoD, right) by these checkpoints are reduced to 2-dimension via t-SNE [22], showing clearly the resulting 3 isolated modes.

(a) InD data, test set, **mode-1**. (b) InD data, test set, **mode-2**. (c) InD data, test set, **mode-3**.

(d) OoD data set, **mode-1**. (e) OoD data set, **mode-2**. (f) OoD data set, **mode-3**.
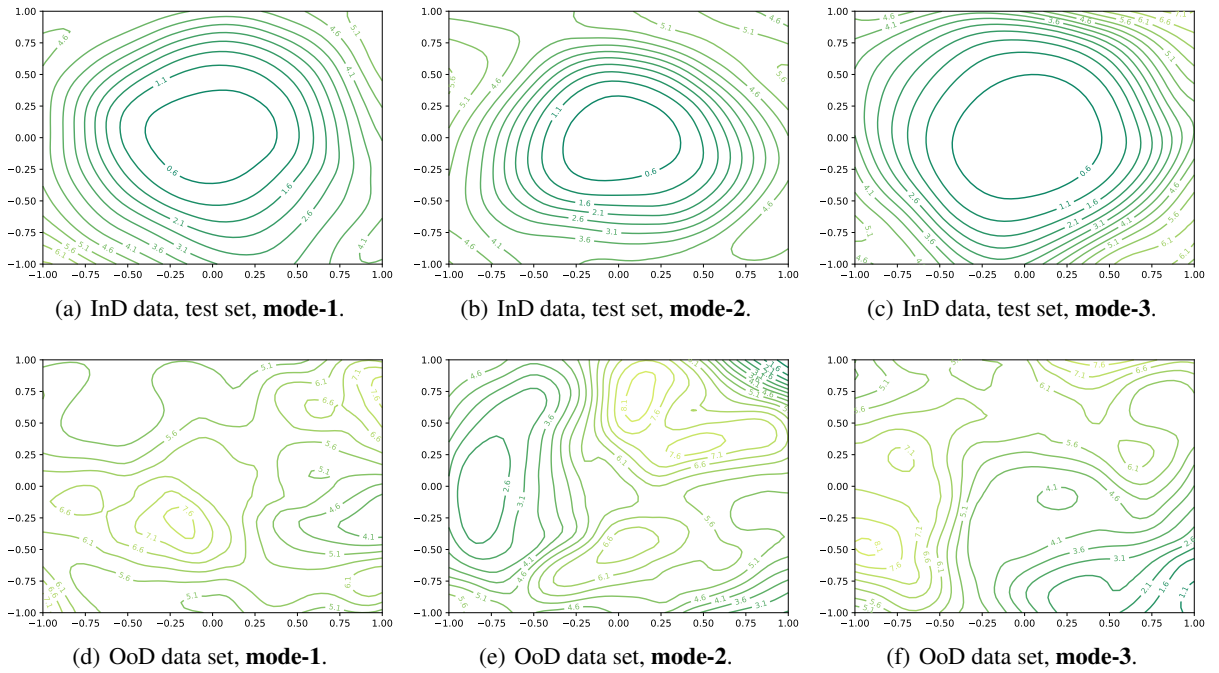
Figure 4: An illustration of the loss landscapes of 3 independent modes (left, middle and right, respectively) on the InD (top) and OoD (bottom) data. The visualization technique follows [23].

As these modes are well-trained on the InD data, though they are independent and isolated with each other, their locations in the loss landscape of InD data still share similarities, *i.e.*, low-loss regions of the InD data. However, for the unseen data from an *out* distribution, these modes might be located in distinct positions with either high or low losses on the OoD data. In Fig.4, as a complement to Fig.1, the loss landscapes of each mode on the InD and OoD data are visualized, and there clearly exist notable differences in the OoD loss landscapes among those independent modes.

Accordingly, the diversities on the loss landscapes (Fig.4) and features (Fig.3) among the independent modes inspire us to investigate the OoD detection problem across such modes. As the existing OoD detectors mainly focus on one single mode and rely on the differences in the logits or features between InD and OoD data, a hypothesis naturally comes to the mind:

The OoD detection performance of one single mode is of high uncertainty, since such a mode, well-trained on InD data, is possibly located in diverse positions of significantly different loss landscapes of OoD data.

4

Our experiments in Sec.3 and Appendix D further validate this hypothesis, *i.e.*, the high variances of the OoD detection performance across independent modes.

Such a phenomenon has not been explored by the research community. The high variances among independent modes hinder the development and evaluation of OoD detectors. In this regard, we hope our work could benefit OoD detection researches from the perspective of independent modes in the loss landscape, as an alternative aside from exploiting the outputs of single DNNs.

2.2.2 Mode ensemble

To further exploit such diversities on the OoD loss landscape and to reduce the high variances across modes, we revisit the deep ensemble method [20], leverage multiple independent modes to perform mode ensemble, and find significant variance reduction with substantial performance improvements in OoD detection.

Nevertheless, how to efficiently involve various OoD detection methods into the mode ensemble framework remains a troublesome issue. On the one hand, as pointed in [24], directly ensembling the "yes or no" detection results from multiple single modes will accumulate the misclassification probabilities. On the other hand, current detectors work on different outputs of DNNs, including logits, features and gradients, which indicates that the mode ensemble should be carefully designed for specific detectors.

Given N modes $f_{s_1}, \cdots, f_{s_N} : \mathbb{R}^D \to \mathbb{R}^C$ trained independently *w.r.t* N random seeds $s_1, \cdots, s_N$, in this work, the mode ensemble during inference takes a general form as:

$$\boldsymbol{h}_{\text{ens}} = \frac{1}{N} \sum_{i=1}^{N} \boldsymbol{h}_{s_i}, \tag{2}$$

where $\boldsymbol{h}_{s_i}$ denotes the output features or logits from f_{s_i}. Such ensembled features or logits $\boldsymbol{h}_{\text{ens}}$ from multiple isolated modes are then exploited by different OoD detectors to achieve mode ensemble for OoD detection. We put complete and thorough details of the mode ensemble for representative OoD detectors in Appendix A. In this work, we mainly focus on those *post-hoc* and *OoD-agnostic* detectors, covering all aforementioned 3 types, since such detectors do not require OoD data nor additional model modifications during training, and execute detection strategies only in the inference stage.

Discussions with other ensemble methods for OoD detection [25, 26, 24] Among these works, [25] requires training DNNs with a margin loss involving additional OoD data, which is orthogonal to our settings that models trained solely on InD data are considered. [26] introduces the contrastive loss and the triplet loss to train Siamese networks and triplet networks for ensemble, where the trained networks are not independent with each other. In [24], a novel p-value-based ensemble strategy is proposed for detecting OoD samples, which differs from the common threshold-based decision rule. Our loss landscape perspective motivates us to focus on the general case: standard models trained without OoD data, in correspondence to those post-hoc, OoD-agnostic and model-agnostic OoD detectors.

2.3 Theoretical analysis

In this section, we provide a theoretical discussion on how ensemble boosts OoD detection performance. Our analysis follows the setups in [27] and shows the superiority of ensembling modes over the average of single modes in terms of accuracy difference between InD data and OoD data.

Let us consider a binary classification problem and suppose the in distribution $\mathcal{P}_{\text{in}}$ is an isotropic Gaussian:

$$\mathcal{P}_{\text{in}} = \{(\boldsymbol{x}, y) \mid \boldsymbol{x} \sim \mathcal{N}(\boldsymbol{\mu} \cdot y; \sigma^2 \boldsymbol{I}_{D \times D})\}, \tag{3}$$

with $\boldsymbol{x} \in \mathbb{R}^D$, $y \in \{-1, 1\}$, the mean vector $\boldsymbol{\mu} \in \mathbb{R}^D$ and the variance σ^2 ($\sigma > 0$). The out distribution $\mathcal{P}_{\text{out}}$ is defined as a shift from $\mathcal{P}_{\text{in}}$:

$$\mathcal{P}_{\text{out}} = \{(\boldsymbol{x}, y) \mid \boldsymbol{x} \sim \mathcal{N}(\boldsymbol{\mu}' \cdot y; \sigma'^2 \boldsymbol{I}_{D \times D}), \quad \boldsymbol{\mu}' = \alpha \cdot \boldsymbol{\mu} + \beta \cdot \boldsymbol{\Delta}, \sigma' = \gamma \cdot \sigma\}, \tag{4}$$

where $\alpha, \beta, \gamma > 0$ are fixed scalars and $\boldsymbol{\Delta} \in \mathbb{R}^D$ is an unknown random distribution.

For mode ensemble, we consider N linear classifiers in the form of $g_i : \boldsymbol{x} \to \text{sign}(\boldsymbol{\theta}_i^\top \boldsymbol{x}), i = 1, \cdots, N$, learned *w.r.t* N different random seeds on $\mathcal{P}_{\text{in}}$, each with weights $\boldsymbol{\theta}_i \in \mathbb{R}^D$. The mode ensemble function is thus defined as $g_{\text{ens}} : \boldsymbol{x} \to \text{sign}(\sum_{i=1}^{N}(\boldsymbol{\theta}_i^\top \boldsymbol{x}))$. The following proposition states the superiority of mode ensemble in achieving a lower gap on the accuracy between InD data and OoD data over the average of multiple modes.

mode	mode-1	mode-2	mode-3	mode-4	mode-5
InD Acc.	74.25	74.30	74.46	74.29	74.33

Table 1: The classification accuracy on the ImageNet-1K validation set of 5 isolated modes of DenseNet121.

Proposition 1. *Consider the in distribution* $\mathcal{P}_{\mathrm{in}}$, *out distribution* $\mathcal{P}_{\mathrm{out}}$, *and N independent modes* $g_i, i = 1, \cdots, N$ *defined above, we have* $\mathcal{G}(g_{\mathrm{ens}}, \mathcal{P}_{\mathrm{in}}, \mathcal{P}_{\mathrm{out}}) \leq \frac{1}{N} \sum_{i=1}^{N} \mathcal{G}(g_i, \mathcal{P}_{\mathrm{in}}, \mathcal{P}_{\mathrm{out}})$, *where*

$$\mathcal{G}(g, \mathcal{P}_{\mathrm{in}}, \mathcal{P}_{\mathrm{out}}) = \left| \Phi^{-1}(\mathcal{ACC}(g, \mathcal{P}_{\mathrm{out}})) - \frac{\alpha}{\gamma} \Phi^{-1}(\mathcal{ACC}(g, \mathcal{P}_{\mathrm{in}})) \right| \tag{5}$$

denotes the gap of the probit-transformed accuracy between $\mathcal{P}_{\mathrm{in}}$ *and* $\mathcal{P}_{\mathrm{out}}$ *achieved by the classifier g.* Φ^{-1} *indicates the inverse of the standard normal cumulative distribution function* $\Phi(x) = \int_{-\infty}^{x} \frac{1}{\sqrt{2\pi}} e^{-t^2/2} \mathrm{d}t$.

The proof of this proposition is deferred to Appendix C. In the next section, extensive empirical results will verify the high variances on the OoD detection performance among independently trained models on InD data, and the substantial improvements brought by mode ensemble.

3 Experiments

In experiments, we will empirically show (i) the high variances of independent modes on the OoD detection performance in Sec.3.2, (ii) the substantial improved detection results via mode ensemble in Sec.3.3, and (iii) more in-depth empirical discussions on the mode ensemble in Sec.3.4.

3.1 Setups

Following previous works on OoD detection [3, 4, 5, 6, 8, 9, 1, 10, 11, 12, 13], our experiments are executed on the small-scale CIFAR10 [28] and the large-scale ImageNet-1K [29] benchmarks. To obtain multiple isolated modes, for the former, 10 models are independently trained on CIFAR10 *w.r.t* 10 different random seeds, including structures of ResNet18 [30] and Wide ResNet28x10 [31]. For the latter, 5 models of ResNet50 [30] and DenseNet121 [32] are independently trained *w.r.t* 5 different random seeds on ImageNet-1K. We further train 3 independent models of T2T-ViT-14 [33] *w.r.t* 3 different random seeds from scratch on ImageNet-1K to further evaluate the mode performance on such a transformer structure.

For CIFAR10 as the InD data, we evaluate the OoD detection performance of different modes on 5 OoD data sets: SVHN [34], LSUN [35], iSUN [36], Textures [37] and Places [38]. For ImageNet-1K as the InD data, the selected OoD data sets include iNaturalist [39], SUN [40], Places [38] and Textures [37]. Refer to Appendix B.1 for details of these data sets.

We select 7 representative and SOTA OoD detectors as the baselines, including MSP [3], ODIN [4], Energy [6], Mahalanobis [5], KNN [11], RankFeat [1] and GradNorm [9]. These are all post-hoc and OoD-agnostic detectors, covering logits-based (MSP, ODIN, Energy), features-based (Mahalanobis, KNN and RankFeat) and gradients-based (GradNorm) types. We evaluate the detection performance of these methods on multiple independent modes to show the high detection variances existing widely in different types of detectors and network structures, and then perform mode ensemble to reduce the variances and boost OoD detection performance. For each single and ensembling modes, we record their (i) InD classification accuracy, (ii) false positive rate (FPR) on OoD data sets when the true positive rate on InD data is 95% and (iii) area under the receiver operating characteristic curve (AUROC).

Remark For checkable reproducibility, all the training and evaluation code and the trained checkpoints are released[1] publicly. The details of model training can also be found in Appendix B.2. Besides, for a clear elaboration, in the following Sec.3.2 and Sec.3.3, we mainly present results of DenseNet121 and ViT on ImageNet-1K and the 6 common detectors, including 3 logits-based (MSP, ODIN and Energy), 1 gradients-based (GradNorm), and 2 features-based (Mahalanobis and RankFeat) detectors. Comprehensive results covering more modes on other InD and OoD datasets, baseline detectors and network structures are provided in Appendix D.

---

[1]https://github.com/fanghenshaometeor/ood-mode-ensemble

Modes	OoD data sets							
	iNaturalist		SUN		Places		Textures	
	FPR↓	AUROC↑	FPR↓	AUROC↑	FPR↓	AUROC↑	FPR↓	AUROC↑
MSP								
mode-1	58.44	87.18	**71.11**	80.78	**74.11**	**79.69**	67.07	80.72
mode-2	**55.68**	**87.28**	**68.78**	**81.49**	**70.85**	**80.63**	66.21	80.27
mode-3	58.29	87.10	70.60	81.02	73.01	80.07	66.06	80.70
mode-4	58.52	87.20	70.73	80.81	72.79	79.77	67.85	80.46
mode-5	60.97	86.19	70.82	80.69	72.76	79.89	64.41	80.93
ODIN								
mode-1	54.88	89.39	60.26	85.76	65.84	83.33	54.36	86.61
mode-2	50.56	90.21	55.79	87.00	60.81	85.08	53.35	86.62
mode-3	51.61	90.12	57.90	86.08	63.82	85.08	53.35	86.62
mode-4	51.47	90.26	59.03	86.28	63.56	84.01	55.12	86.20
mode-5	58.13	88.39	59.17	85.84	63.17	84.07	51.83	86.19
Energy								
mode-1	56.24	88.63	57.85	85.99	64.35	83.29	51.93	86.98
mode-2	52.86	89.67	53.31	87.32	59.77	85.16	50.76	87.05
mode-3	53.19	89.61	55.89	86.35	62.05	84.13	50.64	86.86
mode-4	53.31	89.77	56.85	86.58	62.75	84.08	53.56	86.53
mode-5	60.92	87.56	56.76	86.07	61.93	84.11	49.93	86.46
GradNorm								
mode-1	73.79	77.93	72.64	75.03	81.21	70.23	66.15	77.82
mode-2	69.99	79.89	68.30	76.72	75.71	72.63	63.30	78.74
mode-3	69.93	79.67	69.12	77.56	77.22	73.34	64.06	78.48
mode-4	66.85	81.07	72.51	75.61	80.08	71.44	65.87	77.27
mode-5	77.07	73.47	73.66	73.88	80.59	69.90	66.83	76.39
Mahalanobis								
mode-1	89.20	63.79	84.50	70.98	83.84	71.65	43.56	75.46
mode-2	93.31	60.90	85.98	68.14	83.87	71.11	65.21	58.26
mode-3	88.43	69.11	86.21	70.74	85.17	72.50	51.40	70.16
mode-4	91.84	58.88	86.82	66.23	85.54	69.64	49.86	68.64
mode-5	92.43	59.27	82.07	70.24	81.02	72.95	57.20	63.21
RankFeat								
mode-1	66.01	85.91	75.53	80.27	79.95	75.64	43.60	90.35
mode-2	58.49	83.77	34.70	92.02	50.70	86.12	32.73	92.45
mode-3	59.53	85.17	50.07	88.37	63.27	82.05	40.64	91.54
mode-4	84.70	78.61	69.57	83.82	76.45	78.21	49.89	90.81
mode-5	46.58	87.27	44.46	88.42	58.95	81.54	22.48	94.15

Table 2: The detection performance of each independent mode (DenseNet121 trained on ImageNet-1K) on each OoD data set *w.r.t* different types of OoD detectors. The **best** and worst of the detection results among the 5 modes are highlighted.

3.2 High variances among the independent modes for OoD detection

This subsection empirically presents the existence of a high variance in the OoD detection results of multiple isolated modes. The classification accuracy of these modes on the InD data is shown in Tab.1 to illustrate that these modes are all well-trained on InD data. Then, regarding the OoD detection, the detection results of each mode *w.r.t* different detectors are reported in Tab.2.

In Tab.2, we mark the **best** and worst FPR and AUROC results of the 5 modes on each OoD data set achieved by each OoD detector. Though these modes all perform consistently well on the InD data in Tab.1, there clearly exists a large variance of the OoD detection results across independent modes for different detectors. Specifically, we can find the following two phenomena.

Ensemble	OoD data sets							
of k modes	iNaturalist		SUN		Places		Textures	
	FPR↓	AUROC↑	FPR↓	AUROC↑	FPR↓	AUROC↑	FPR↓	AUROC↑
MSP								
$k=1$	58.38±1.87	86.99±0.45	70.41±0.93	80.96±0.32	72.70±1.17	80.01±0.37	66.32±1.29	80.62±0.26
$k=2$	54.69±1.01	88.29±0.24	68.75±0.39	82.03±0.04	70.72±0.37	81.21±0.12	64.05±0.57	81.58±0.05
$k=3$	53.57±0.55	88.75±0.19	68.31±0.21	82.18±0.09	70.74±0.37	81.38±0.12	63.39±0.48	**81.99±0.02**
$k=4$	**53.42±0.49**	**88.94±0.11**	**68.48±0.15**	**82.34±0.01**	**70.47±0.35**	**81.52±0.06**	**63.35±0.78**	82.11±0.07
ODIN								
$k=1$	53.33±3.14	89.67±0.80	58.43±1.70	86.19±0.50	63.44±1.80	84.31±0.76	53.51±1.28	86.43±0.22
$k=2$	50.60±2.55	91.06±0.56	56.50±1.54	87.37±0.40	61.09±0.96	85.47±0.46	49.41±0.93	**88.30±0.06**
$k=3$	48.43±0.89	91.76±0.15	**55.75±0.35**	**87.62±0.11**	60.59±0.49	**85.78±0.16**	**47.49±0.22**	88.86±0.14
$k=4$	**48.37±0.28**	**91.93±0.09**	55.81±0.50	87.74±0.14	**60.62±0.46**	85.89±0.20	46.52±0.57	89.13±0.08
Energy								
$k=1$	55.30±3.42	89.05±0.95	56.13±1.72	86.46±0.53	62.17±1.65	84.15±0.66	51.36±1.42	86.78±0.27
$k=2$	51.33±1.78	90.85±0.46	53.75±1.14	87.64±0.22	59.90±1.54	85.44±0.48	46.00±1.18	88.83±0.11
$k=3$	49.58±1.60	91.52±0.28	52.72±1.04	88.05±0.20	58.84±1.19	85.93±0.33	44.27±0.51	**89.48±0.03**
$k=4$	**49.23±0.97**	**91.64±0.20**	**52.33±0.27**	**88.23±0.07**	**58.34±0.57**	**86.14±0.10**	**42.74±0.43**	89.81±0.08
GradNorm								
$k=1$	71.53±3.96	78.41±2.98	71.25±2.38	75.76±1.44	78.96±2.38	71.51±1.49	65.24±1.49	77.74±0.95
$k=2$	69.97±3.93	79.96±2.53	68.72±1.53	77.06±0.94	77.15±1.67	72.93±1.08	61.93±0.88	79.85±0.41
$k=3$	67.58±2.53	81.99±1.44	67.78±0.41	77.97±0.32	76.43±0.49	73.69±0.27	60.71±0.75	**81.05±0.19**
$k=4$	**67.22±1.64**	**82.33±0.93**	**66.65±0.22**	**78.44±0.26**	**75.37±0.14**	**74.33±0.23**	**59.59±0.41**	81.52±0.21
Mahalanobis								
$k=1$	91.04±2.12	62.39±4.22	85.12±1.90	69.27±2.03	83.89±1.77	71.57±1.30	53.45±8.17	67.15±6.61
$k=2$	88.68±2.96	**65.43±2.15**	**83.44±3.27**	72.48±4.09	**83.41±2.78**	73.45±2.57	44.60±8.88	75.07±5.99
$k=3$	83.25±6.50	72.39±3.72	82.77±5.00	76.03±4.03	83.83±3.40	74.50±2.54	**37.22±7.31**	**82.91±4.23**
$k=4$	**81.49±2.78**	72.42±2.48	82.59±4.45	**76.15±3.11**	84.14±3.55	**74.44±2.07**	39.01±7.63	81.81±5.44
RankFeat								
$k=1$	63.06±13.98	84.15±3.34	54.87±17.18	86.58±4.57	65.86±12.20	80.71±3.99	37.87±10.59	91.86±1.51
$k=2$	49.18±13.04	89.67±2.61	45.30±11.30	89.80±2.57	59.64±8.77	83.70±2.61	23.21±2.71	**95.04±0.10**
$k=3$	45.78±10.18	90.96±1.93	43.45±3.39	90.57±0.82	**58.07±2.18**	84.49±0.69	**18.98±0.51**	95.98±0.25
$k=4$	**40.92±5.41**	**91.82±0.99**	**38.68±3.01**	**91.51±0.52**	54.84±2.31	**85.38±0.49**	16.44±0.77	96.43±0.36

Table 3: The detection performance of ensembling k independent modes (DenseNet121 trained on ImageNet-1K) on each OoD data set *w.r.t* different types of OoD detectors. Results with the **lowest variances** are highlighted with bold fonts.

- For the same OoD detector, independent modes hold significantly-fluctuating FPR results. For example, the RankFeat [1] even reaches a worst FPR value 84.71% by the mode-4 and a best FPR value 46.58% by the mode-5 on the iNaturalist [39] data set.

- For different modes, detection results among those methods might be opposite. For example, considering the mode-4, Energy [6] achieves better detection result on iNaturalist (53.31%) than RankFeat (84.70%), while for the mode-5, RankFeat (46.58%) outperforms Energy (60.92%) a lot on iNaturalist.

Such widely-existed high variances support our viewpoint: *The OoD detection performance of single modes is of high uncertainty*. In addition, these phenomena are more conspicuous on the small-scale CIFAR10 benchmark with even higher variances of the detection FPR results across independent modes, see Appendix D for complete results and more analysis.

3.3 Mode ensemble stabilizes and boosts OoD detection

In this subsection, mode ensemble is introduced to alleviate the high variances of the OoD detection performance among multiple isolated modes and to further boost the detection. Table 3 shows the OoD detection performance of ensembling k modes. For $k = 1$, we record the mean values and standard deviations of the detection results among the total N modes. For each $k > 1$, firstly k different modes are randomly selected and get ensembled to perform OoD detection, then such process is repeated 3 times to calculate the mean values and standard deviations of the detection results of ensembling k modes.

As shown in Tab.3, regarding the aforementioned 2 phenomena in the preceding subsection, we can find:

- For the same OoD detector, mode ensemble could significantly reduce the detection variances and substantially improve the detection performance. For example, the mean FPR results of RankFeat [1] on iNaturalist [39] get improved from 63.06% to 40.92% with a variance reduction from 13.98 to 5.41.

- Such rather stable detection results brought by mode ensemble also benefit the evaluation of those OoD detectors and get rid of the uncertainties of single modes.

In addition, one can find disparities in performance enhancement brought by mode ensemble on different OoD detectors. RankFeat and Mahalanobis [5] exhibit considerable improvements, while MSP [3], ODIN [4] and Energy [6] only show modest gains. The reasons behind lie in the different types of these OoD detectors: features-based (RankFeat and Mahalanobis) and logits-based (MSP, ODIN and Energy). The features of DNNs are generally viewed as latent representations of the inputs in a latent space, and thereby can contain richer information than the final logits of DNNs, as the latter is computed as the probabilities distributed on the classification categories. In this way, for multiple isolated modes of DNNs, the features learned by these modes can be more diverse and informative than the logits of these modes. Accordingly, ensembling these features for Mahalanobis and RankFeat is naturally superior than ensembling these logits for MSP, ODIN and Energy, leading to the more substantial performance improvements

The advantages of mode ensemble, *i.e.*, variance reduction and performance improvements, are also widely reflected on the small-scale CIFAR10 benchmark for different types of OoD detectors. Refer to Appendix D for thorough results on mode ensemble for OoD detection.

Modes	OoD data sets							
	iNaturalist		SUN		Places		Texture	
	FPR↓	AUROC↑	FPR↓	AUROC↑	FPR↓	AUROC↑	FPR↓	AUROC↑
	MSP							
mode-1	**48.22**	**88.99**	**65.21**	81.89	**68.26**	**80.15**	61.72	82.45
mode-2	47.41	89.27	**64.98**	**82.13**	68.69	80.39	**61.13**	**82.40**
mode-3	**44.52**	**89.78**	65.12	**81.82**	**67.32**	**80.75**	61.88	82.63
AVG. single	46.72±1.95	89.35±0.40	65.10±0.12	81.95±0.16	68.09±0.70	80.43±0.30	61.58±0.40	82.49±0.12
AVG. ensemble	**42.70±0.92**	**90.86±0.24**	**64.38±0.39**	**82.75±0.10**	**67.29±0.26**	**81.42±0.13**	**57.54±0.39**	**84.35±0.11**
	ODIN							
mode-1	**45.30**	**87.41**	**64.34**	**77.42**	68.26	**73.78**	56.58	81.29
mode-2	44.66	88.08	64.29	**78.09**	**69.36**	74.68	**56.74**	**81.25**
mode-3	**41.28**	**89.07**	**63.77**	77.80	**66.46**	**75.38**	**56.29**	**81.90**
AVG. single	43.75±2.16	88.19±0.84	64.13±0.32	77.77±0.34	68.03±1.46	74.61±0.80	56.54±0.23	81.48±0.36
AVG. ensemble	**38.63±1.15**	**91.00±0.35**	**63.37±0.28**	**79.77±0.17**	**66.94±0.33**	**76.93±0.36**	**50.82±0.45**	**85.01±0.19**
	Energy							
mode-1	57.93	81.43	73.11	69.69	76.81	64.47	58.58	78.54
mode-2	**62.35**	**80.82**	**74.59**	**69.15**	**79.12**	64.42	60.82	**77.95**
mode-3	**57.47**	**83.55**	**73.06**	**70.37**	**76.06**	**66.72**	**57.62**	**79.39**
AVG. single	59.25±2.69	81.93±1.43	73.59±0.87	69.74±0.61	77.33±1.59	65.20±1.31	59.01±1.64	78.63±0.72
AVG. ensemble	**49.00±0.74**	**88.20±0.43**	**70.37±0.28**	**74.26±0.22**	**73.55±0.38**	**69.95±0.55**	**48.39±0.20**	**84.76±0.26**
	Mahalanobis							
mode-1	**94.92**	**54.64**	**96.43**	**45.48**	**97.14**	43.48	**91.13**	**60.91**
mode-2	**99.64**	**37.76**	**98.23**	**35.07**	**98.84**	**34.48**	**84.06**	**62.94**
mode-3	98.15	39.87	97.48	45.17	97.78	**44.37**	87.15	61.77
AVG. single	97.57±2.41	44.09±9.20	97.38±0.90	41.91±5.92	97.92±0.86	40.78±5.47	87.45±3.54	61.87±1.02
AVG. ensemble	**94.52±4.31**	**52.82±10.02**	**95.70±1.85**	**49.63±6.81**	**96.71±1.10**	**47.61±6.62**	**84.52±9.02**	**64.46±10.17**
	RankFeat							
mode-1	63.71	85.64	74.30	75.72	74.05	74.66	67.48	**75.24**
mode-2	**69.54**	**80.87**	**78.46**	**75.06**	**83.74**	**70.18**	**52.41**	**85.63**
mode-3	**61.25**	**86.64**	**71.18**	**78.52**	**71.55**	**77.38**	68.05	75.98
AVG. single	64.83±4.26	84.38±3.08	74.65±3.65	76.43±1.84	76.45±6.44	74.07±3.64	62.65±8.87	78.95±5.80
AVG. ensemble	**54.06±5.83**	**89.33±1.03**	**70.91±2.56**	**80.19±1.58**	**72.19±1.20**	**78.17±1.01**	**55.77±7.63**	**83.15±4.02**

Table 4: The detection performance of each of the 3 modes of T2T-ViT-14 trained from scratch on ImageNet-1K *w.r.t* 5 OoD detectors: MSP, ODIN, Energy, Mahalanobis and RankFeat. The **best** and worst results of each mode are highlighted.

Results on ViT models In recent years, the Vision Transformer (ViT, [21]) has been a powerful network structure in various tasks [41]. Therefore, experiments on ViT models are executed to further verify our observations on the

performance of isolated modes in OoD detection. Table 4 illustrates the detection performance of both single modes and mode ensemble ($k = 2$), where each single mode is of T2T-ViT-14 [33] and trained on ImageNet-1K [29] from scratch.

As shown in Tab.4, due to the powerful generalization ability of T2T-ViT-14, there exist even smaller detection variances of multiple isolated modes, especially for those logits-based detectors (MSP [3], ODIN [4] and Energy [6]). Even though, those features-based detectors, especially RankFeat [1], still hold very high variances among independent modes. On the other hand, mode ensemble always brings variance reduction and substantial performance improvements for different OoD detectors. In short, results in Tab.4 again validate the high detection variances of single modes and the substantial improvements of mode ensemble in the case of ViT models.

3.4 In-depth empirical discussions on mode ensemble

3.4.1 On the independence of ensembling modes

Ablation studies are provided to show that the ensemble of those modes, which are from the same trajectory and thus are not independent, can not bring OoD detection performance improvements.

Setups Given a well-trained mode f_{s_n} with parameters $\boldsymbol{\omega}_{s_n} \in \mathbb{R}^K$ *w.r.t* a random seed s_n, we obtain M modes $f_{s_n}^{(i)}, i = 1, \cdots, M$ by sampling from the subspace of f_{s_n} as follows:

$$\boldsymbol{\omega}_{s_n}^{(i)} = \boldsymbol{\omega}_{s_n} + r \cdot \frac{\boldsymbol{u}}{\|\boldsymbol{u}\|}, i = 1, \cdots, M, \tag{6}$$

where $\boldsymbol{u} \in \mathcal{N}(0^K, 1^K)$ and r denotes a random step size. In this way, the obtained M modes $f_{s_n}^{(i)}$ are not independent with each other and are concentrated around f_{s_n}. Comparison results between ensembling such modes and ensembling the independent modes on InD recognition accuracy and OoD detection FPR values are shown in Fig.5.

Results As shown in Fig.5, on the one hand, mode ensemble could bring higher InD accuracy and lower OoD FPR values for both the 2 types of modes that are isolated with each other or are all sampled from the same subspace. On the other hand, ensembling those independent modes clearly shows better generalization performance on InD data and stronger detection performance on OoD data than ensembling those modes that are not isolated. From the perspective of loss landscape, those isolated modes *w.r.t* different trajectories hold much more diversified information than those modes concentrated around the same trajectory, thereby leading to better ensemble performance in both InD generalization and OoD detection.
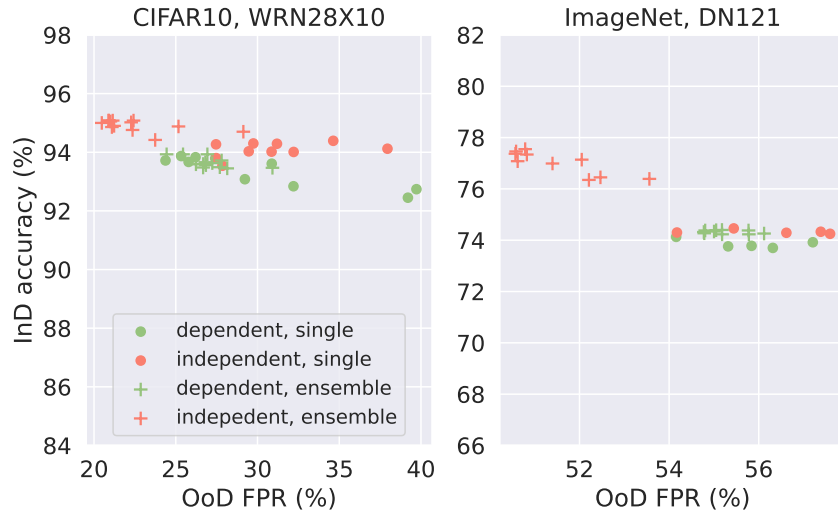

Figure 5: Ablation studies on the independence of modes. Each data point indicates the results of one single mode (circle dots) or ensembled modes (plus markers) with InD accuracy (y-axis) and average detection FPR over multiple OoD data sets (x-axis) achieved by Energy [6].

10

3.4.2 On the model capacity of ensembling modes

Aside from the enhanced detection performance, ensembling multiple modes simultaneously increases model capacities. Therefore, it is meaningful to compare the performance of the mode ensemble with single models having an equivalent number of parameters, in order to provide insights into whether increasing model complexity is a viable alternative to enhancing OoD detection. Accordingly, we design the following experiments on CIFAR10 and ImageNet-1K benchmarks.

Setups   As shown in Tab.5 below, when taking CIFAR10 [28] as the InD data, the number of parameters of the three ResNet18 (RN18, [30]) networks is nearly equivalent with that of one Wide ResNet28X10 (WRN28X10, [31]) network. When taking ImageNet-1K [29] as the InD data, the number of parameters of three DenseNet121 (DN121, [32]) networks is nearly equivalent with that of one ResNet50 (RN50, [30]) network. Therefore, in the experiments, the detection performance of ensembling $k = 3$ modes of RN18 and DN121 is compared with that of a single WRN28X10 and RN50, respectively, whose detailed results are given in Tab.6 and Tab.7.

data set	network	# of modes	total capacity
CIFAR10	RN18	$k = 3$	11,173,962 $\times$3
	WRN28X10	$k = 1$	36,489,290
ImageNet-1K	RN50	$k = 1$	25,557,032
	DN121	$k = 3$	7,978,856 $\times$3

Table 5: Model capacities of different network structures.

Results   Taking the detection results on the large-scale ImageNet-1K benchmark in Tab.6 as an example, despite the similar numbers of parameters, increasing model complexity does not necessarily guarantee the enhancement of OoD detection performance, which varies across different data sets and OoD detectors.

- For the GradNorm detector [9], a single mode of RN50 generally outperforms the ensemble of three modes of DN121 in detection performance under all the OoD data sets.

- Meanwhile, for the other detectors, especially the RankFeat [1], the ensemble of three DN121 exhibits much better OoD detection performance than that of the single RN50.

The detection results on the small-scale CIFAR10 benchmark shown in Tab.7 also present similar phenomena. In short, simply increasing the model capacities cannot necessarily bring OoD detection performance improvements, as the detection performance is affected by multiple factors, such as the network structures, the tested OoD data, and the chosen detectors and ensemble strategies.

3.4.3 On the sensitivity of the number of ensembling modes

DNNs with different structures have distinctive loss landscapes on OoD data, which can affect the detection performance when ensembling isolated modes in such loss landscapes. Thus, for different DNN structures, the chosen number of modes, *i.e.*, k, can lead to varied performance boosts by the mode ensemble. Accordingly, we further investigate the effects on k under different DNN structures through the following experiments.

Setups   Varying numbers of ensembling modes k are considered in experiments, and the corresponding detection performance brought by ensembling such modes is recorded under different DNN structures. RN18 and WRN28X10 structures are taken for CIFAR10, while DN121 and T2T-ViT-14 structures are used for ImageNet-1K. For the OoD detection in the experiments, we adopt the widely used and effective detection method Energy [6].

Results   Figure 6 shows the mean and standard deviations of the FPR results from different DNN structures on CIFAR10 and ImageNet-1K benchmarks, as the number of ensembling modes k increases.

- On the CIFAR10 benchmark, RN18 and WRN28X10 do not exhibit significant differences *w.r.t* the FPR metric in relation to the number of ensembling modes k.
  In this experiment, the detection performance trending among the tested different DNN structures shows to be similar along with the variation of k.

- On the ImageNet-1K benchmark, as k increases, the FPR drop, *i.e.*, the performance boost, varies distinctively between DN121 and T2T-ViT-14. In Fig.6, the FPR values of the ViT-based structure (T2T-ViT-14) decrease

Ensemble	OoD data sets							
of k modes	iNaturalist		SUN		Places		Textures	
	FPR↓	AUROC↑	FPR↓	AUROC↑	FPR↓	AUROC↑	FPR↓	AUROC↑
MSP								
$k=1$ RN50	56.86±1.76	87.50±0.45	70.75±0.55	80.92±0.30	72.65±0.25	80.32±0.12	68.01±1.48	80.45±0.61
$k=3$ DN121	53.63±0.79	88.76±0.16	68.58±0.45	82.18±0.14	70.63±0.33	81.35±0.20	63.53±1.01	81.97±0.21
ODIN								
$k=1$ RN50	54.09±1.52	90.04±0.32	59.67±0.75	86.47±0.44	63.73±0.79	84.74±0.28	55.95±1.69	85.81±0.64
$k=3$ DN121	48.15±1.95	91.84±0.34	55.86±1.16	87.64±0.20	60.90±0.82	85.71±0.26	47.88±0.26	88.89±0.11
Energy								
$k=1$ RN50	57.14±1.45	89.38±0.32	57.78±1.05	86.75±0.47	62.56±0.64	84.83±0.31	54.18±1.72	86.03±0.66
$k=3$ DN121	49.65±1.88	91.43±0.41	52.68±1.03	88.03±0.22	58.96±0.69	85.87±0.28	43.95±0.52	89.53±0.11
GradNorm								
$k=1$ RN50	56.87±4.22	83.87±1.71	64.23±2.37	79.38±1.15	72.42±1.49	75.28±0.86	60.02±2.96	79.25±1.23
$k=3$ DN121	67.11±2.43	82.20±1.35	67.24±1.86	78.15±0.99	75.91±1.78	73.96±1.04	60.40±1.28	81.09±0.57
Mahalanobis								
$k=1$ RN50	96.74±1.01	51.44±5.63	96.84±0.39	50.57±2.00	96.29±0.37	51.84±1.10	43.02±7.89	78.30±8.48
$k=3$ DN121	83.08±3.89	71.71±5.53	82.28±4.06	75.31±2.27	83.55±3.54	74.49±1.74	41.35±4.06	79.32±2.80
RankFeat								
$k=1$ RN50	87.91±8.24	63.17±11.47	82.25±6.77	73.38±7.74	85.79±5.13	68.94±6.86	63.83±9.05	79.96±5.41
$k=3$ DN121	44.81±7.92	91.20±1.76	43.12±6.57	90.69±1.54	57.94±5.27	84.66±1.61	18.95±1.85	96.01±0.52

Table 6: Comparisons on the detection performance between single modes and mode ensemble with nearly equivalent numbers of parameters on the **ImageNet-1K** benchmark.

Ensemble	OoD data sets									
of k modes	SVHN		LSUN		iSUN		Texture		Places365	
	FPR↓	AUROC↑	FPR↓	AUROC↑	FPR↓	AUROC↑	FPR↓	AUROC↑	FPR↓	AUROC↑
MSP										
$k=1$ WRN28X10	44.79±9.78	93.87±1.37	26.32±4.66	96.32±0.48	49.01±7.75	93.11±1.32	58.35±5.00	89.75±1.35	59.82±2.04	88.93±0.62
$k=3$ RN18	67.09±3.11	88.48±1.74	46.83±3.00	93.28±0.58	55.09±1.26	92.02±0.60	58.36±1.13	90.59±0.31	59.05±1.38	89.32±0.10
ODIN										
$k=1$ WRN28X10	25.83±10.93	95.66±1.82	5.52±1.25	98.91±0.20	24.38±5.94	95.98±0.78	47.00±6.76	89.81±2.12	44.65±4.41	90.45±1.16
$k=3$ RN18	63.47±6.93	88.10±2.63	20.70±2.43	96.50±0.49	28.57±5.71	95.54±1.04	47.65±1.47	90.89±0.56	43.30±0.68	90.81±0.16
Energy										
$k=1$ WRN28X10	25.36±11.32	95.76±1.80	5.97±1.23	98.84±0.21	29.65±7.06	95.32±1.03	48.56±6.76	89.61±2.05	44.89±4.51	90.50±1.14
$k=3$ RN18	65.98±7.65	87.95±2.66	20.14±2.82	96.59±0.52	29.59±5.64	95.31±1.12	48.16±1.91	90.99±0.59	42.14±0.23	91.05±0.13
Mahalanobis										
$k=1$ WRN28X10	12.07±18.53	97.30±3.94	73.88±7.96	76.89±4.60	6.77±1.87	98.26±0.60	24.54±8.47	92.46±3.18	85.08±2.29	69.46±2.21
$k=3$ RN18	9.02±5.92	97.37±2.16	74.67±4.59	75.73±1.54	27.88±14.34	88.04±8.41	36.54±19.94	84.24±14.08	86.43±1.56	71.38±3.43
KNN										
$k=1$ WRN28X10	23.35±4.76	96.46±0.63	20.23±2.34	96.74±0.36	26.87±7.25	95.62±1.18	36.07±5.58	94.15±0.98	46.43±3.07	90.44±0.76
$k=3$ RN18	47.12±2.53	93.12±0.75	51.46±2.88	92.19±0.59	29.92±2.14	95.46±0.43	36.35±0.58	94.15±0.30	53.74±0.89	89.38±0.14

Table 7: Comparisons on the detection performance between single modes and mode ensemble with nearly equivalent numbers of parameters on the **CIFAR10** benchmark.

more sharply than that of the DenseNet-based structure (DN121), where T2T-ViT-14 requires fewer numbers of modes for ensemble to achieve competitive or even better detection performances than DN121. It is also noticed that as k increases, the standard deviation (the shaded area) of FPR from ensembling modes of T2T-ViT-14 shows to be much smaller than that from ensembling modes of DN121, which indicates *(i)* the stronger robustness of ViT agianst OoD and *(ii)* the decreased uncertainties with larger k.

In this experiment, the detection performance trending between the ViT and the DN121 differs in the varied FPR drops and the standard deviations of FPR along with increasing k, where fewer k of ensembling ViT yields more performance boosts.

3.4.4 On ensembling modes of different model structures

In this section, a discussion on ensembling modes of different structures is provided. When it comes to different types of OoD detectors, such as the *features*-based detector and the *logits*-based ones, there are several technical points to be taken into account for the ensemble.
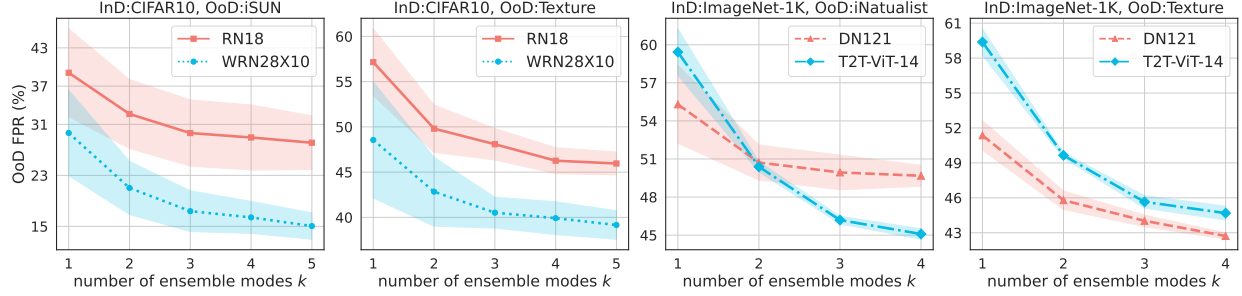
12

Figure 6: FPR of different DNN structures on CIFAR10 and ImageNet-1K benchmarks under varied numbers of ensembling modes k. The shaded area indicates the standard deviations of FPR values of ensembling different modes.

Ensemble of k modes	OoD data sets									
	SVHN		LSUN		iSUN		Texture		Places365	
	FPR↓	AUROC↑	FPR↓	AUROC↑	FPR↓	AUROC↑	FPR↓	AUROC↑	FPR↓	AUROC↑
$k = 1$ RN18	62.67	88.40	22.73	96.02	39.92	92.96	49.54	90.37	45.73	89.64
$k = 1$ WRN28X10	21.94	96.38	3.85	99.21	25.64	95.86	8.51	92.12	47.43	90.18
ENSEMBLE	27.49	95.60	6.09	98.76	19.66	96.81	36.05	93.54	40.28	91.77

Table 8: Experiments on ensembling two modes of different structures (RN18 and WRN28X10) under the Energy detector on the CIFAR10 benchmark.

- For detectors relying on the *logits* of DNNs to determine the detection score, *e.g.*, the Energy [6], it is convenient to directly ensemble the logits from different network structures, *e.g.*, a ResNet50 and a DenseNet121, since the outputs logits from the ResNet50 and the DenseNet121 hold the same dimension, and denote the probability distributions over the classification categories.

- For detectors relying on the *features* of DNNs to proceed the detection, *e.g.*, the KNN detector [11], the ensemble requires the same dimensionality of the utilized features from different structures, *e.g.*, a ResNet50 and a DenseNet121. Besides, as features extracted by the ResNet50 and the DenseNet121 actually indicate distinctive representations in their own latent spaces, ensembling such features might not guarantee detection performance improvements.

In the following Tab.8 and Tab.9, we present two examples of ensembling two modes of different network structures under the Energy detector [6] (logits-based) on the CIFAR10 and ImageNet-1K benchmarks. Detection performance improvements are also maintained by the mode ensemble on several OoD data sets. Such mode ensemble for different structures can be easily extended to other detectors using logits to determine the detection score, such as MSP [3], ODIN [4] and RankFeat [1]. While for the detectors using features to calculate detection scores, *e.g.*, the KNN detector [11], the penultimate features from the RN18 and WRN28X10 backbone have different dimensions, *i.e.*, 512 for RN18 and 640 for WRN28X10, the KNN detector cannot be proceeded in the mode ensemble, neither can another Mahalanobis detector [5] evaluated in our work.

3.4.5 Comparisons with other ensemble detectors

In the ablation studies in Sec.3.4.1, we have compared the detection performance between ensembling independent modes and dependent ones. In this section, the proposed mode ensemble is further compared with another type of ensemble for OoD detection: ZODE [24]. Different from ensembling the output logits or features in DNNs of our method, ZODE proposes to perform ensemble on the p-values from multiple models, where the p-values are calculated from the detection scores. Accordingly, the key difference between our mode ensemble and ZODE is,

- In ours, the outputs (logits or features) from multiple modes are firstly get ensembled, then the detection score is computed based on the ensembled outputs to decide OoD predictions.

- In ZODE, the detection score of each individual model is firstly determined to calculate the p-value, then those p-values from multiple models get ensembled to decide OoD predictions.

13

Ensemble of k modes	OoD data sets							
	iNaturalist		SUN		Places		Textures	
	FPR↓	AUROC↑	FPR↓	AUROC↑	FPR↓	AUROC↑	FPR↓	AUROC↑
$k = 1$ RN50	56.06	89.64	56.88	87.37	61.85	85.21	55.53	85.63
$k = 1$ DN121	52.86	89.67	53.31	87.32	59.77	85.16	50.76	87.05
ENSEMBLE	50.41	91.31	52.41	88.54	57.95	86.49	47.64	88.64

Table 9: Experiments on ensembling two modes of different structures (RN50 and DN121) under the Energy detector on the ImageNet-1K benchmark.

Table 10 and Table 11 present the comparison results in OoD detection between ZODE [24] and ours on ImageNet-1K and CIFAR10 benchmarks, respectively. For fair comparisons, in each experiment, the k modes for ensemble in our method are exactly the same models utilized in ZODE. These k models are randomly selected under each OoD detector, whose indices are also listed in the tables.

As shown in Tab.10 and Tab.11, under different OoD detectors and different numbers of ensembled models, our mode ensemble method generally outperforms ZODE in terms of the average FPR values on multiple OoD data sets. Such results indicate that ensembling the output features or logits from multiple DNNs might be a better choice than ensembling the scores from multiple DNNs in OoD detection, since features or logits could contain more useful and diversified information than the decision scores.

Ensemble of k modes	Method	OoD data sets									
		iNaturalist		SUN		Places		Textures		**AVERAGE**	
		FPR↓	AUROC↑	FPR↓	AUROC↑	FPR↓	AUROC↑	FPR↓	AUROC↑	FPR↓	AUROC↑
		MSP									
$k = 2$	ZODE	56.40	**88.68**	69.63	**82.28**	71.70	**81.43**	63.58	**82.75**	65.33	**83.79**
(mode-2,5)	ours	**55.85**	88.01	**68.44**	81.99	**70.78**	81.21	**63.42**	81.60	**64.62**	83.20
$k = 4$	ZODE	56.02	**90.00**	70.80	**82.81**	73.45	**81.89**	64.13	**83.96**	66.10	**84.67**
(mode-1,2,3,4)	ours	**52.86**	89.06	**68.65**	82.35	**70.81**	81.54	**63.99**	82.06	**64.08**	83.75
		ODIN									
$k = 2$	ZODE	57.13	90.15	60.61	86.79	65.24	84.69	51.70	88.22	58.67	87.46
(mode-1,5)	ours	**52.77**	**90.58**	**58.28**	**86.92**	**62.15**	**84.94**	**49.17**	**88.37**	**55.59**	**87.70**
$k = 4$	ZODE	56.38	91.65	60.86	87.82	65.70	85.93	51.45	**89.06**	58.60	88.62
(mode-2,3,4,5)	ours	**48.04**	**92.03**	**55.26**	**87.88**	**60.09**	**86.07**	**46.93**	89.05	**52.58**	**88.76**
		Energy									
$k = 2$	ZODE	57.55	89.78	55.38	87.72	61.16	85.67	47.62	88.65	55.43	87.96
(mode-2,5)	ours	**53.22**	**90.39**	**52.64**	**87.88**	**58.32**	**85.94**	**44.66**	**88.86**	**52.21**	**88.27**
$k = 4$	ZODE	56.27	91.12	57.95	88.08	64.50	85.79	48.42	89.61	56.79	88.65
(mode-1,2,3,4)	ours	**48.14**	**91.84**	**52.26**	**88.25**	**58.87**	**86.08**	**43.07**	**89.85**	**50.59**	**89.01**
		Mahalanobis									
$k = 2$	ZODE	92.00	61.54	88.50	68.85	87.45	71.05	44.40	74.42	78.09	68.97
(mode-1,4)	ours	**87.65**	**65.43**	**81.10**	**74.54**	**81.20**	**75.02**	**39.43**	**78.06**	**72.35**	**73.26**
$k = 4$	ZODE	94.10	62.72	90.77	69.80	89.58	72.23	46.17	74.44	80.16	69.80
(mode-1,3,4,5)	ours	**79.60**	**71.33**	**77.54**	**79.12**	**80.09**	**76.72**	**33.16**	**85.21**	**67.60**	**78.10**

Table 10: Comparisons between ZODE and ours on ensembling k modes (**DenseNet121** trained on **ImageNet-1K**) on each OoD data set *w.r.t* different OoD detectors.

4 Related work

4.1 OoD detection

The task of OoD detection focuses on the detection ability of DNNs on data from an out distribution $\mathcal{P}_{\text{out}}$ differing from the training distribution [42]. Plenty of researches have been developed from various aspects, see reviews in [14, 15].

Aside from the outlined 3 types of detectors, logits-based, features-based and gradients-based, in Sec.1, which are mainly post-hoc and OoD-agnostic, there exist other detectors that work on the training process via additional data or

Ensemble of k modes	Method	OoD data sets											
		SVHN		LSUN		iSUN		Texture		Places365		**AVERAGE**	
		FPR↓	AUROC↑	FPR↓	AUROC↑	FPR↓	AUROC↑	FPR↓	AUROC↑	FPR↓	AUROC↑	FPR↓	AUROC↑
		MSP											
$k=2$	ZODE	74.47	**86.91**	50.68	92.90	52.44	**93.08**	62.57	**90.06**	62.22	88.89	60.48	90.37
(mode-2,8)	ours	**72.64**	86.88	**49.05**	**93.12**	**51.88**	92.98	**61.15**	90.01	**60.08**	**89.09**	**58.96**	**90.42**
$k=4$	ZODE	69.85	89.49	**44.71**	**93.67**	49.76	**93.28**	58.24	**91.23**	58.77	89.50	56.27	**91.43**
(mode-4,6,7,8)	ours	**64.69**	**89.58**	45.34	93.54	52.96	92.49	**57.36**	91.05	**58.21**	**89.53**	**55.71**	91.24
		ODIN											
$k=2$	ZODE	75.74	83.48	**23.52**	**96.13**	**34.53**	**95.05**	54.36	89.57	48.14	**89.91**	47.26	**90.83**
(mode-3,7)	ours	**72.86**	**83.66**	24.70	95.75	36.90	94.65	**50.92**	**89.93**	**47.31**	89.81	**46.64**	90.76
$k=4$	ZODE	75.50	88.98	**16.60**	**97.57**	**21.89**	**97.01**	51.93	91.63	45.72	**91.36**	42.33	93.31
(mode-6,7,8,9)	ours	**63.13**	**89.78**	**15.36**	97.30	23.08	96.42	**44.10**	**91.87**	**40.80**	91.34	**37.29**	**93.34**
		Energy											
$k=2$	ZODE	72.76	**87.78**	24.31	**96.36**	27.22	96.00	58.09	90.03	48.01	90.48	46.08	**92.13**
(mode-4,8)	ours	**71.68**	87.22	**21.85**	96.31	**23.84**	**96.03**	**51.05**	**90.43**	**44.08**	**90.60**	**42.50**	92.12
$k=4$	ZODE	72.85	88.73	23.14	**96.63**	39.98	94.67	55.32	91.38	47.53	91.03	47.76	92.49
(mode-3,4,6,7)	ours	**61.06**	**89.30**	**19.83**	96.55	**33.65**	**94.80**	**44.91**	**91.76**	**41.44**	**91.13**	**40.18**	**92.71**
		Mahalanobis											
$k=2$	ZODE	21.73	95.53	64.32	84.29	**11.94**	**96.49**	50.82	**76.88**	86.90	69.68	47.14	**84.57**
(mode-1,7)	ours	**17.55**	**95.59**	**55.33**	**86.17**	14.10	95.36	59.33	69.93	87.60	**69.93**	**46.78**	83.40
$k=4$	ZODE	14.17	97.36	69.28	82.88	6.26	98.73	29.26	93.17	88.44	70.70	41.46	**88.57**
(mode-1,3,6,7)	ours	**4.65**	**98.90**	76.00	74.98	10.57	97.66	**28.17**	91.00	**86.71**	**73.34**	41.22	87.18

Table 11: Comparisons between ZODE and ours on ensembling k modes (**ResNet18** trained on **CIFAR10**) on each OoD data set *w.r.t* different OoD detectors.

model modifications. For example, G-ODIN [43] designs a two-branch network structure to decompose the output probabilities and to alleviate the over-confidence on OoD data. An auto-encoder is introduced for OoD detection in an unsupervised way with the Stiefel-Restricted Kernel Machine in [44]. [45] discusses 2 different distribution shifts for the out distribution $\mathcal{P}_{\text{out}}$ and proposes semantics information as the detection metric.

Related theoretical works in OoD detection mainly study single modes. A theoretical framework for OoD generalization is formalized in [46]. The probably approximated correct learning theory for OoD detection is investigated in [47]. Our theoretical work discusses the mode ensemble for OoD detection in a simple binary classification problem on Gaussian distributions.

In this work, we discover the uncertainty in OoD evaluations on the loss landscape of isolated modes. Interestingly, [48] also discusses similar unreliability issues in OoD evaluations. Different from our loss landscape perspective, the key viewpoint of [48] is from an image-level view, and a human-centric OoD evaluation metric is proposed to alleviate the difficulty of detecting the distribution shift in input images. Both our work and [48] provide insights on the reliability issues of current OoD evaluations and offer corresponding viable solutions from different aspects.

4.2 Mode, loss landscape and ensemble

Mode and loss landscape　Analyzing the mode properties in the loss landscape of DNNs could date back to [49], which shows that the loss along a straight line connecting the initialization and the final solution monotonically decreases. Then, [17] and [16] find low-loss curves that connect two independent modes in the loss landscape and [19] proposes a training algorithm to learn subspaces of DNNs in the forms of lines, Bezier curves and simplexes. Mode connectivity has also inspired researches in other fields. For example, [50, 51] leverage mode connectivity for more robust DNNs against adversarial examples. [52] proposes weight-averaging on the independent modes for better OoD generalization.

Ensemble　Ensemble has been a useful technique to improve the model generalization performance on the InD test data in both classic machine learning [53] and the deep learning [20]. [18] visualizes and quantitatively measures the functional space diversity in the loss landscape to show how deep ensemble boosts the generalization performance on InD data. Besides, the ensemble technique has been widely utilized in different fields, such as adversarial and certified robustness [54, 55, 56] and machinery fault diagnosis [57].

5 Conclusion and discussion

In this work, starting from the loss landscape perspective, we observe that those independent modes, which are trained to achieve low-loss regions on InD data *w.r.t* different random seeds, yet yield significantly different loss landscapes of

OoD data. The research community has ignored the uncertainties brought by such diversities across isolated modes on the OoD loss landscape: (i) For the same OoD detector, independent modes could hold substantially varied detection performance, and (ii) For two OoD detectors, different modes could yield opposite performance. Accordingly, to alleviate the high variances, we revisit the deep ensemble method to ensemble multiple independent modes so as to achieve stable results and substantially improve detecting OoD data, which also benefits the development and evaluation on OoD detectors in the sense of reduced variances. Our experiments cover different types of OoD detectors, various network structures, small-scale and large-scale data sets with in-depth explorations on many aspects of the mode ensemble, which supports our viewpoint comprehensively and solidly together with the theoretical analysis on the reduced accuracy gap between InD and OoD data.

Nevertheless, the extra computation in training has been an inevitable limitation in ensemble methods, as sequentially training multiple DNNs is time-consuming. One could mitigate this problem via more efficient training tricks, such as the parallel training for the base DNNs. Besides, in the future work, more sophisticated ensemble strategies could be specifically devised for particular OoD detectors, on the basis of the unique properties of the detector and the provided baseline ensemble strategies of our work.

Acknowledgements

References

[1] Yue Song, Nicu Sebe, and Wei Wang. Rankfeat: Rank-1 feature removal for out-of-distribution detection. Advances in Neural Information Processing Systems, 35:17885–17898, 2022.

[2] Chiyuan Zhang, Samy Bengio, Moritz Hardt, Benjamin Recht, and Oriol Vinyals. Understanding deep learning (still) requires rethinking generalization. Communications of the ACM, 64(3):107–115, 2021.

[3] Dan Hendrycks and Kevin Gimpel. A baseline for detecting misclassified and out-of-distribution examples in neural networks. In International Conference on Learning Representations, 2016.

[4] Shiyu Liang, Yixuan Li, and R Srikant. Enhancing the reliability of out-of-distribution image detection in neural networks. In International Conference on Learning Representations, 2018.

[5] Kimin Lee, Kibok Lee, Honglak Lee, and Jinwoo Shin. A simple unified framework for detecting out-of-distribution samples and adversarial attacks. Advances in neural information processing systems, 31, 2018.

[6] Weitang Liu, Xiaoyun Wang, John Owens, and Yixuan Li. Energy-based out-of-distribution detection. Advances in neural information processing systems, 33:21464–21475, 2020.

[7] Jinsol Lee and Ghassan AlRegib. Gradients as a measure of uncertainty in neural networks. In 2020 IEEE International Conference on Image Processing (ICIP), pages 2416–2420. IEEE, 2020.

[8] Yiyou Sun, Chuan Guo, and Yixuan Li. React: Out-of-distribution detection with rectified activations. Advances in Neural Information Processing Systems, 34:144–157, 2021.

[9] Rui Huang, Andrew Geng, and Yixuan Li. On the importance of gradients for detecting distributional shifts in the wild. Advances in Neural Information Processing Systems, 34:677–689, 2021.

[10] Yao Zhu, YueFeng Chen, Chuanlong Xie, Xiaodan Li, Rong Zhang, Hui Xue, Xiang Tian, Yaowu Chen, et al. Boosting out-of-distribution detection with typical features. Advances in Neural Information Processing Systems, 35:20758–20769, 2022.

[11] Yiyou Sun, Yifei Ming, Xiaojin Zhu, and Yixuan Li. Out-of-distribution detection with deep nearest neighbors. In International Conference on Machine Learning, pages 20827–20840. PMLR, 2022.

[12] Haoqi Wang, Zhizhong Li, Litong Feng, and Wayne Zhang. Vim: Out-of-distribution with virtual-logit matching. In Proceedings of the IEEE/CVF Conference on Computer Vision and Pattern Recognition, pages 4921–4930, 2022.

[13] Yeonguk Yu, Sungho Shin, Seongju Lee, Changhyun Jun, and Kyoobin Lee. Block selection method for using feature norm in out-of-distribution detection. In Proceedings of the IEEE/CVF Conference on Computer Vision and Pattern Recognition, pages 15701–15711, 2023.

[14] Jingkang Yang, Kaiyang Zhou, Yixuan Li, and Ziwei Liu. Generalized out-of-distribution detection: A survey. International Journal of Computer Vision, pages 1–28, 2024.

[15] Zheyan Shen, Jiashuo Liu, Yue He, Xingxuan Zhang, Renzhe Xu, Han Yu, and Peng Cui. Towards out-of-distribution generalization: A survey. arXiv preprint arXiv:2108.13624, 2021.

[16] Timur Garipov, Pavel Izmailov, Dmitrii Podoprikhin, Dmitry P Vetrov, and Andrew G Wilson. Loss surfaces, mode connectivity, and fast ensembling of dnns. Advances in neural information processing systems, 31, 2018.

[17] Felix Draxler, Kambis Veschgini, Manfred Salmhofer, and Fred Hamprecht. Essentially no barriers in neural network energy landscape. In International conference on machine learning, pages 1309–1318. PMLR, 2018.

[18] Stanislav Fort, Huiyi Hu, and Balaji Lakshminarayanan. Deep ensembles: A loss landscape perspective. arXiv preprint arXiv:1912.02757, 2019.

[19] Mitchell Wortsman, Maxwell C Horton, Carlos Guestrin, Ali Farhadi, and Mohammad Rastegari. Learning neural network subspaces. In International Conference on Machine Learning, pages 11217–11227. PMLR, 2021.

[20] Balaji Lakshminarayanan, Alexander Pritzel, and Charles Blundell. Simple and scalable predictive uncertainty estimation using deep ensembles. Advances in neural information processing systems, 30, 2017.

[21] Alexey Dosovitskiy, Lucas Beyer, Alexander Kolesnikov, Dirk Weissenborn, Xiaohua Zhai, Thomas Unterthiner, Mostafa Dehghani, Matthias Minderer, Georg Heigold, Sylvain Gelly, et al. An image is worth 16x16 words: Transformers for image recognition at scale. In International Conference on Learning Representations, 2020.

[22] Laurens van der Maaten and Geoffrey Hinton. Visualizing data using t-sne. Journal of Machine Learning Research, 9:2579–2605, 2008.

[23] Hao Li, Zheng Xu, Gavin Taylor, Christoph Studer, and Tom Goldstein. Visualizing the loss landscape of neural nets. Advances in neural information processing systems, 31, 2018.

[24] Feng Xue, Zi He, Chuanlong Xie, Falong Tan, and Zhenguo Li. Boosting out-of-distribution detection with multiple pre-trained models. arXiv preprint arXiv:2212.12720, 2022.

[25] Apoorv Vyas, Nataraj Jammalamadaka, Xia Zhu, Dipankar Das, Bharat Kaul, and Theodore L Willke. Out-of-distribution detection using an ensemble of self supervised leave-out classifiers. In Proceedings of the European Conference on Computer Vision (ECCV), pages 550–564, 2018.

[26] Donghun Yang, Kien Mai Ngoc, Iksoo Shin, Kyong-Ha Lee, and Myunggwon Hwang. Ensemble-based out-of-distribution detection. Electronics, 10(5):567, 2021.

[27] John P Miller, Rohan Taori, Aditi Raghunathan, Shiori Sagawa, Pang Wei Koh, Vaishaal Shankar, Percy Liang, Yair Carmon, and Ludwig Schmidt. Accuracy on the line: on the strong correlation between out-of-distribution and in-distribution generalization. In International Conference on Machine Learning, pages 7721–7735. PMLR, 2021.

[28] A Krizhevsky. Learning multiple layers of features from tiny images. Master's thesis, University of Toronto, 2009.

[29] Jia Deng, Wei Dong, Richard Socher, Li-Jia Li, Kai Li, and Li Fei-Fei. Imagenet: A large-scale hierarchical image database. In Proceedings of the IEEE Conference on Computer Vision and Pattern Recognition, pages 248–255, 2009.

[30] Kaiming He, Xiangyu Zhang, Shaoqing Ren, and Jian Sun. Deep residual learning for image recognition. In IEEE Conference on Computer Vision and Pattern Recognition, pages 770–778, 2016.

[31] Sergey Zagoruyko and Nikos Komodakis. Wide residual networks. In British Machine Vision Conference 2016. British Machine Vision Association, 2016.

[32] Gao Huang, Zhuang Liu, Laurens Van Der Maaten, and Kilian Q Weinberger. Densely connected convolutional networks. In Proceedings of the IEEE conference on computer vision and pattern recognition, pages 4700–4708, 2017.

[33] Li Yuan, Yunpeng Chen, Tao Wang, Weihao Yu, Yujun Shi, Zi-Hang Jiang, Francis EH Tay, Jiashi Feng, and Shuicheng Yan. Tokens-to-token vit: Training vision transformers from scratch on imagenet. In Proceedings of the IEEE/CVF international conference on computer vision, pages 558–567, 2021.

[34] Yuval Netzer, Tao Wang, Adam Coates, Alessandro Bissacco, Bo Wu, and Andrew Y Ng. Reading digits in natural images with unsupervised feature learning. In Proceedings of the NIPS Workshop on Deep Learning and Unsupervised Feature Learning, 2011.

[35] Fisher Yu, Ari Seff, Yinda Zhang, Shuran Song, Thomas Funkhouser, and Jianxiong Xiao. Lsun: Construction of a large-scale image dataset using deep learning with humans in the loop. arXiv preprint arXiv:1506.03365, 2015.

17

[36] Pingmei Xu, Krista A Ehinger, Yinda Zhang, Adam Finkelstein, Sanjeev R Kulkarni, and Jianxiong Xiao. Turkergaze: Crowdsourcing saliency with webcam based eye tracking. arXiv preprint arXiv:1504.06755, 2015.

[37] Mircea Cimpoi, Subhransu Maji, Iasonas Kokkinos, Sammy Mohamed, and Andrea Vedaldi. Describing textures in the wild. In Proceedings of the IEEE Conference on Computer Vision and Pattern Recognition, pages 3606–3613, 2014.

[38] Bolei Zhou, Agata Lapedriza, Aditya Khosla, Aude Oliva, and Antonio Torralba. Places: A 10 million image database for scene recognition. IEEE transactions on pattern analysis and machine intelligence, 40(6):1452–1464, 2017.

[39] Grant Van Horn, Oisin Mac Aodha, Yang Song, Yin Cui, Chen Sun, Alex Shepard, Hartwig Adam, Pietro Perona, and Serge Belongie. The inaturalist species classification and detection dataset. In Proceedings of the IEEE conference on computer vision and pattern recognition, pages 8769–8778, 2018.

[40] Jianxiong Xiao, James Hays, Krista A Ehinger, Aude Oliva, and Antonio Torralba. Sun database: Large-scale scene recognition from abbey to zoo. In 2010 IEEE computer society conference on computer vision and pattern recognition, pages 3485–3492. IEEE, 2010.

[41] William Peebles and Saining Xie. Scalable diffusion models with transformers. In Proceedings of the IEEE/CVF International Conference on Computer Vision, pages 4195–4205, 2023.

[42] Anh Nguyen, Jason Yosinski, and Jeff Clune. Deep neural networks are easily fooled: High confidence predictions for unrecognizable images. In Proceedings of the IEEE conference on computer vision and pattern recognition, pages 427–436, 2015.

[43] Yen-Chang Hsu, Yilin Shen, Hongxia Jin, and Zsolt Kira. Generalized odin: Detecting out-of-distribution image without learning from out-of-distribution data. In Proceedings of the IEEE/CVF Conference on Computer Vision and Pattern Recognition, pages 10951–10960, 2020.

[44] Francesco Tonin, Arun Pandey, Panagiotis Patrinos, and Johan AK Suykens. Unsupervised energy-based out-of-distribution detection using stiefel-restricted kernel machine. In 2021 International Joint Conference on Neural Networks (IJCNN), pages 1–8. IEEE, 2021.

[45] Jingkang Yang, Kaiyang Zhou, and Ziwei Liu. Full-spectrum out-of-distribution detection. International Journal of Computer Vision, pages 1–16, 2023.

[46] Haotian Ye, Chuanlong Xie, Tianle Cai, Ruichen Li, Zhenguo Li, and Liwei Wang. Towards a theoretical framework of out-of-distribution generalization. Advances in Neural Information Processing Systems, 34:23519–23531, 2021.

[47] Zhen Fang, Yixuan Li, Jie Lu, Jiahua Dong, Bo Han, and Feng Liu. Is out-of-distribution detection learnable? Advances in Neural Information Processing Systems, 35:37199–37213, 2022.

[48] Yao Zhu, Yuefeng Chen, Xiaodan Li, Rong Zhang, Hui Xue, Xiang Tian, Rongxin Jiang, Bolun Zheng, and Yaowu Chen. Rethinking out-of-distribution detection from a human-centric perspective. International Journal of Computer Vision, pages 1–18, 2024.

[49] Ian J Goodfellow, Oriol Vinyals, and Andrew M Saxe. Qualitatively characterizing neural network optimization problems. In International Conference on Learning Representations, 2015.

[50] Pu Zhao, Pin-Yu Chen, Payel Das, Karthikeyan Natesan Ramamurthy, and Xue Lin. Bridging mode connectivity in loss landscapes and adversarial robustness. In International Conference on Learning Representations, 2020.

[51] Ren Wang, Yuxuan Li, and Sijia Liu. Exploring diversified adversarial robustness in neural networks via robust mode connectivity. In Proceedings of the IEEE/CVF Conference on Computer Vision and Pattern Recognition, pages 2345–2351, 2023.

[52] Alexandre Rame, Matthieu Kirchmeyer, Thibaud Rahier, Alain Rakotomamonjy, Patrick Gallinari, and Matthieu Cord. Diverse weight averaging for out-of-distribution generalization. Advances in Neural Information Processing Systems, 35:10821–10836, 2022.

[53] Zhi-Hua Zhou. Ensemble methods: foundations and algorithms. CRC press, 2012.

[54] Kun Fang, Qinghua Tao, Yingwen Wu, Tao Li, Jia Cai, Feipeng Cai, Xiaolin Huang, and Jie Yang. Towards robust neural networks via orthogonal diversity. Pattern Recognition, 149:110281, 2024.

[55] Miklós Z Horváth, Mark Niklas Mueller, Marc Fischer, and Martin Vechev. Boosting randomized smoothing with variance reduced classifiers. In International Conference on Learning Representations, 2021.

[56] Kun Fang, Qinghua Tao, Yingwen Wu, Tao Li, Xiaolin Huang, and Jie Yang. On multi-head ensemble of smoothed classifiers for certified robustness. arXiv preprint arXiv:2211.10882, 2022.

[57] Te Han and Yan-Fu Li. Out-of-distribution detection-assisted trustworthy machinery fault diagnosis approach with uncertainty-aware deep ensembles. Reliability Engineering & System Safety, 226:108648, 2022.

[58] Mitchell Wortsman, Gabriel Ilharco, Samir Ya Gadre, Rebecca Roelofs, Raphael Gontijo-Lopes, Ari S Morcos, Hongseok Namkoong, Ali Farhadi, Yair Carmon, Simon Kornblith, et al. Model soups: averaging weights of multiple fine-tuned models improves accuracy without increasing inference time. In International conference on machine learning, pages 23965–23998. PMLR, 2022.

Appendix A   Baseline OoD detectors and mode ensemble

We outline how the scoring function $S(\cdot)$ is designed in the selected baseline OoD detectors and elaborate the corresponding mode ensemble strategies over these detectors. In the following, the outputs of the mode $f : \mathbb{R}^D \to \mathbb{R}^C$ are the logits of C-dimension, in correspondence to C classes.

MSP [3] takes the maximum probability over the output logits as the scoring function. Given a new sample $\boldsymbol{x} \in \mathbb{R}^D$, its MSP score *w.r.t* a single mode $f(\cdot)$ is

$$S_{\mathrm{MSP}}(\boldsymbol{x}) = \max\left(\mathrm{softmax}(f(\boldsymbol{x}))\right). \tag{7}$$

Ensemble on MSP adopts the average logits from N modes $f_{s_i}, i = 1, \cdots, N$ to calculate the maximum probability as the score for $\boldsymbol{x}$:

$$S_{\mathrm{MSP\text{-}ens}}(\boldsymbol{x}) = \max\left(\mathrm{softmax}\left(\frac{1}{N}\sum_{i=1}^{N} f_{s_i}(\boldsymbol{x})\right)\right). \tag{8}$$

ODIN [4] introduces temperature scaling and adversarial examples into MSP and proposes the following score:

$$S_{\mathrm{ODIN}}(\boldsymbol{x}) = \max\left(\mathrm{softmax}(\frac{f(\bar{\boldsymbol{x}})}{T})\right), \tag{9}$$

where T denotes the temperature and $\bar{\boldsymbol{x}}$ denotes the perturbed adversarial example of $\boldsymbol{x}$. Following the settings in [4, 1], we set $T = 1000$ and do not perturb $\boldsymbol{x}$ for the ImageNet-1K benchmark in experiments.

Ensemble on ODIN shares a similar scoring function with that of MSP-ensemble:

$$S_{\mathrm{ODIN\text{-}ens}}(\boldsymbol{x}) = \max\left(\mathrm{softmax}(\frac{\sum_{i=1}^{N} f_{s_i}(\bar{\boldsymbol{x}})}{N \cdot T})\right). \tag{10}$$

The adversarial attack is executed individually on each mode f_{s_i} and then the ODIN score is calculated on the average predictive logits on the perturbed inputs.

Energy [6] improves MSP via an energy function since energy is better aligned with the input probability density:

$$S_{\mathrm{energy}}(\boldsymbol{x}) = \log\sum_{i=1}^{C} \exp(f^i(\boldsymbol{x})), \tag{11}$$

where $f^i(\boldsymbol{x})$ denotes the i-th element in the C-dimension output logits.

Ensemble on Energy firstly averages the N logits and then computes the energy score:

$$S_{\mathrm{energy\text{-}ens}}(\boldsymbol{x}) = \log\sum_{i=1}^{C} \exp(f_{\mathrm{ens}}^i(\boldsymbol{x})), \quad f_{\mathrm{ens}}(\boldsymbol{x}) = \frac{1}{N}\sum_{i=1}^{N} f_{s_i}(\boldsymbol{x}). \tag{12}$$

Mahalanobis [5] tries to model the network outputs at different layers as the mixture of multivariate Gaussian distributions and uses the Mahalanobis distance as the scoring function:

$$S_{\mathrm{mahal}}(\boldsymbol{x}) = \max_{c}\left(-(f(\boldsymbol{x}) - \boldsymbol{\mu}_c)^\top \Sigma (f(\boldsymbol{x}) - \boldsymbol{\mu}_c)\right), \tag{13}$$

where $\boldsymbol{\mu}_c$ denotes the mean feature vector of class-c and Σ denotes the covariance matrix across classes. In experiments, following the settings in [5, 1], adversarial examples generated from 500 randomly-selected clean samples are involved to train the logistic regression, with a perturbation size 0.05 on CIFAR10 and 0.001 on ImageNet-1K.

Ensemble on Mahalanobis leverages the average output features at the same layers in DNNs over N modes and attacks the N modes simultaneously to calculate the Mahalanobis score. Details can be found in the released code.

KNN [11] is a simple but time-consuming and memory-inefficient detector since it performs nearest neighbor search on the ℓ_2-normalized penultimate features between the test sample and all the training samples. The negative of the (k-th) shortest ℓ_2 distance between the features $\boldsymbol{h}^*$ of a new sample $\boldsymbol{x}^*$ and all the training features $\boldsymbol{h}^i$ is set as the score:

$$S_{\mathrm{KNN}}(\boldsymbol{x}^*) = -\min_{i:1,\cdots,n_{\mathrm{tr}}}\left\|\frac{\boldsymbol{h}^*}{\|\boldsymbol{h}^*\|_2} - \frac{\boldsymbol{h}^i}{\|\boldsymbol{h}^i\|_2}\right\|_2, \tag{14}$$

where $\boldsymbol{h}$ denotes the penultimate features in the DNN, and $\boldsymbol{h}^i$ denotes the penultimate features in correspondence to the i-th training sample in the training set of size n_{tr}. The key of this detector is the ℓ_2 normalization on the features.

Ensemble on KNN improves performance by replacing the penultimate features from one single mode with the average penultimate features from N nodes:

$$S_{\text{KNN-ens}}(\boldsymbol{x}^*) = - \min_{j:1,\cdots,n_{\text{tr}}} \left\| \frac{\sum_{i=1}^N \boldsymbol{h}_{s_i}^*}{\| \sum_{i=1}^N \boldsymbol{h}_{s_i}^* \|_2} - \frac{\sum_{i=1}^N \boldsymbol{h}_{s_i}^j}{\| \sum_{i=1}^N \boldsymbol{h}_{s_i}^j \|_2} \right\|_2. \tag{15}$$

RankFeat [1] removes the rank-1 matrix from each individual sample feature matrix $\mathbf{X}$ in the mini-batch during forward propagation in test, since the rank-1 feature drastically perturbs the predictions on OoD samples:

$$\begin{aligned} \mathbf{X} &= \mathbf{U}\mathbf{S}\mathbf{V}^\top, \\ \mathbf{X}' &= \mathbf{X} - \boldsymbol{s}_1 \boldsymbol{u}_1 \boldsymbol{v}_1^\top. \end{aligned} \tag{16}$$

In Eq.(16), the singular value decomposition is firstly executed on the feature matrix $\mathbf{X}$ of an individual sample, leading to the left and right orthogonal singular vector matrices $\mathbf{U}$ and $\mathbf{V}$, and the rectangle diagonal singular value matrix $\mathbf{S}$. Then, the rank-1 matrix is calculated based on the largest singular value $\boldsymbol{s}_1$ and the two corresponding singular vectors $\boldsymbol{u}_1$ and $\boldsymbol{v}_1$, and gets subtracted from the original $\mathbf{X}$. Such removals are recommended at the 3rd and 4th blocks in DNNs. Finally, an Energy score [6] is calculated on the resulting changed output logits.

Ensemble on RankFeat executes the rank-1 feature removing on each mode individually and then average the N changed logits to compute the Energy score as Eq.(12). Details can be found in the released code.

GradNorm [9] leverages the gradient information for OoD detection by calculating the ℓ_1 norm of the gradients *w.r.t* a KL divergence loss as the score of $\boldsymbol{x}$:

$$S_{\text{GN}}(\boldsymbol{x}) = \left\| \frac{\partial \, \text{KL}(\boldsymbol{u} \, \| \, \text{softmax}(f(\boldsymbol{x})))}{\partial \, \boldsymbol{\omega}} \right\|_1, \tag{17}$$

where $\boldsymbol{u} = [1/C, \cdots, 1/C] \in \mathbb{R}^C$ and $\boldsymbol{\omega}$ is set as the weight parameters of the last full-connected layer in DNNs.

Ensemble on GradNorm firstly calculates the KL divergence between $\boldsymbol{u}$ and the softmax probability of the average logits of N modes. The final score for $\boldsymbol{x}$ is the average gradient norm over the selected parameters $\boldsymbol{\omega}_{s_i}$ in each mode:

$$S_{\text{GN-ens}}(\boldsymbol{x}) = \frac{1}{N} \sum_{i=1}^N \left\| \frac{\partial \, \text{KL}(\boldsymbol{u} \, \| \, \text{softmax}(f_{\text{ens}}(\boldsymbol{x})))}{\partial \, \boldsymbol{\omega}_{s_i}} \right\|_1. \tag{18}$$

Appendix B   Experiment setup details

B.1   Details on data sets

The information of the data sets for OoD detection is outlined below. All these settings follow previous works.

For the CIFAR10 benchmark, the InD data is the training and test sets of CIFAR10, with 50,000 and 10,000 $32 \times 32 \times 3$ images of 10 categories, respectively. In this experiment, all images from the OoD data sets are resized to an image size of $32 \times 32 \times 3$. The evaluated OoD data sets are introduced below.

- SVHN [34] data set includes images of street view house numbers. The test set of SVHN is adopted for OoD detection with 26,032 digits of numbers 0-9.
- LSUN [35] data set is about large-scale scene classification and understanding. The test set of LSUN is employed for OoD detection with 10,000 images of 10 categories.
- iSUN [36] data set consists of 8,925 images of gaze traces, all of which are employed for OoD detection.
- Textures [37] data set covers various types of surface texture with 5,640 images of 47 categories. The whole data set is adopted in the evaluation of OoD detection performance.
- Places365 [38] data set is for scene recognition. A subset of 328,500 images are curated for OoD detection by [11].

For the ImageNet-1K benchmark, the InD data is the training and test sets of ImageNet-1K, with 1,281,167 and 50,000 images of 1,000 categories, respectively. In experiments, all images from the OoD data sets are resized to an image size of $224 \times 224 \times 3$. The evaluated OoD data sets are introduced below.

- iNaturalist [39] data set contains natural fine-grained images of different species of plants and animals. For OoD detection, 10,000 images are sampled from the selected concepts by [11].

- SUN [40] data set covers a large variety of environmental scenes, places and the objects within. For OoD detection, 10,000 images are sampled from the selected concepts by [11].

- Places [38] data set is about scene recognition. For OoD detection, 10,000 images are sampled by [11].

- Textures [37] data set in the ImageNet-1K benchmark is the same as that described above in the CIFAR10 benchmark.

data set	network	# GPUs	time per Epoch [s]	total time [h]
CIFAR10	ResNet18	3090 ×1	18.22	0.76
	Wide ResNet28X10	3090 ×1	97.04	4.04
ImageNet-1K	ResNet50	v100 ×4	1950.41	48.76
	DenseNet121	v100 ×4	2439.42	60.99
	T2T-ViT-14	v100 ×8	1607.98	138.47

Table 12: Training time consumed by each individual model with specific GPUs in the experiments.

B.2 Details on model training

Thorough training details of the adopted modes for OoD detection are elaborated below. Particularly, to obtain multiple independent modes, it is required to re-train multiple models from scratch on the training sets of CIFAR10 [28] and ImageNet-1K [29] *w.r.t* different random seeds. For checkable reproducibility of the results reported in this paper, all the training and evaluation code and the trained checkpoints can be found in the publicly-released link given in the main text.

For the 10 independent modes of ResNet18 [30] and Wide ResNet28X10 [31] trained on CIFAR10 [28], each DNN is optimized via SGD for 150 epochs with a batch size of 256 and weight decay 10^{-4}. The initial learning rate is 0.1 and reduced via a cosine scheduler to 0 during training. Each DNN is trained on one single NVIDIA GeForce RTX 3090 GPU.

For the 5 independent modes of ResNet50 [30] and DenseNet121 [32] trained from scratch on ImageNet-1K [29], we follow the official training script[2] provided by PyTorch. Each DNN is optimized via SGD for 90 epochs with weight decay 10^{-4}. The initial learning rate is 0.1 and reduced every 30 epochs by a factor of 10. The batch size for training ResNet50 and DenseNet121 is 1000 and 800, respectively. Each training is executed parallely on 4 NVIDIA v100 GPUs.

For the 3 independent modes of T2T-ViT-14 [33] trained from scratch on ImageNet, we follow the training script provided from the official github repository[3] and adopt the default recommendation settings. Each T2T-ViT-14 model is trained parallely on 8 NVIDIA v100 GPUs for 310 epochs with a batch size of 64, an initial learning rate of 5×10^{-4} and weight decay 0.05.

The final models after the training finishes are evaluated for OoD detection in inference.

Computational overhead For training, general ensemble methods inevitably requires extra time and memory expenses in the employed multiple models than that of single-model-based methods [55, 58]. Similarly in our proposed mode ensemble, multiple modes require training multiple DNNs. In Table 12, we provide the time-consuming of training a single model, where our N-mode ensemble takes such training N times. In implementation, we can proceed the training in parallel to reduce the heavy time cost of training sequentially, given with sufficient computation resources. In this way, multiple DNNs could be obtained in the time of training one DNN. Once the models are trained, our OoD detectors are available at hands. Then, they can be used to detect any given data, where only the inference is needed.

Appendix C Theoretical proofs

This section gives the proof of Proposition 1 in the manuscript, which is reiterated as follows.

---

[2]https://github.com/pytorch/examples/tree/main/imagenet
[3]https://github.com/yitu-opensource/T2T-ViT

Proposition 1′. *Consider the in-distribution $\mathcal{P}_{\text{in}}$ and the out-distribution $\mathcal{P}_{\text{out}}$, and the N modes $g_i, i = 1, \cdots, N$, we have $\mathcal{G}(g_{\text{ens}}, \mathcal{P}_{\text{in}}, \mathcal{P}_{\text{out}}) \leq \frac{1}{N} \sum_{i=1}^{N} \mathcal{G}(g_i, \mathcal{P}_{\text{in}}, \mathcal{P}_{\text{out}})$, where*

$$\mathcal{G}(g, \mathcal{P}_{\text{in}}, \mathcal{P}_{\text{out}}) = \left| \Phi^{-1}(\mathcal{ACC}(g, \mathcal{P}_{\text{out}})) - \frac{\alpha}{\gamma} \Phi^{-1}(\mathcal{ACC}(g, \mathcal{P}_{\text{in}})) \right| \tag{19}$$

denotes the gap of the probit-transformed accuracy between $\mathcal{P}_{\text{in}}$ and $\mathcal{P}_{\text{out}}$ achieved by the classifier g.

Proof. Given the in-distribution $\mathcal{P}_{\text{in}}$ defined as a Gaussian distribution $\mathcal{P}_{\text{in}} = \{(\boldsymbol{x}, y) \mid \boldsymbol{x} \sim \mathcal{N}(\boldsymbol{\mu} \cdot y; \sigma^2 I_{D \times D})\}$ with $\boldsymbol{x} \in \mathbb{R}^D$ and $y \in \{-1, 1\}$, and one single mode in the form of a linear classifier $g_i : \boldsymbol{x} \to \text{sign}(\boldsymbol{\theta}_i^T \boldsymbol{x}), i = 1, \cdots, N$, we have

$$\mathcal{ACC}(g_i, \mathcal{P}_{\text{in}}) = \text{Pr}\left(\text{sign}(\boldsymbol{\theta}_i^T \boldsymbol{x}) = y\right) = \text{Pr}\left(y \cdot (\boldsymbol{\theta}_i^T \boldsymbol{x}) > 0\right)$$

$$= \text{Pr}\left(\mathcal{N}\left(\boldsymbol{\theta}_i^T \boldsymbol{\mu}; \|\boldsymbol{\theta}_i\|^2 \sigma^2\right) \geq 0\right) = \text{Pr}\left(\|\boldsymbol{\theta}_i\|\sigma \cdot \mathcal{N}(0;1) \geq -(\boldsymbol{\theta}_i^T \boldsymbol{\mu})\right) = \Phi\left(\frac{\boldsymbol{\theta}_i^T \boldsymbol{\mu}}{\|\boldsymbol{\theta}_i\|\sigma}\right). \tag{20}$$

Similarly, for the out-distribution $\mathcal{P}_{\text{out}}$ defined as a shift from $\mathcal{P}_{\text{in}}$: $\mathcal{P}_{\text{out}} = \{(\boldsymbol{x}, y) \mid \boldsymbol{x} \sim \mathcal{N}(\boldsymbol{\mu}' \cdot y; \sigma'^2 I_{D \times D})\}$ with $\boldsymbol{\mu}' = \alpha \cdot \boldsymbol{\mu} + \beta \cdot \boldsymbol{\Delta}$ and $\sigma' = \gamma \cdot \sigma$, and the mode ensemble function $g_{\text{ens}} : \boldsymbol{x} \to \text{sign}(\sum_{i=1}^{N} (\boldsymbol{\theta}_i^T \boldsymbol{x}))$, we have

$$\mathcal{ACC}(g_i, \mathcal{P}_{\text{out}}) = \Phi\left(\frac{\boldsymbol{\theta}_i^T \boldsymbol{\mu}'}{\|\boldsymbol{\theta}_i\|\sigma'}\right) = \Phi\left(\frac{\alpha}{\gamma} \cdot \frac{\boldsymbol{\theta}_i^T \boldsymbol{\mu}}{\|\boldsymbol{\theta}_i\|\sigma} + \frac{\beta}{\gamma\sigma} \cdot \frac{\boldsymbol{\theta}_i^T \boldsymbol{\Delta}}{\|\boldsymbol{\theta}_i\|}\right),$$

$$\mathcal{ACC}(g_{\text{ens}}, \mathcal{P}_{\text{in}}) = \Phi\left(\frac{\sum_{i=1}^{N}(\boldsymbol{\theta}_i^T \boldsymbol{\mu})}{\|\sum_{i=1}^{N} \boldsymbol{\theta}_i\|\sigma}\right), \tag{21}$$

$$\mathcal{ACC}(g_{\text{ens}}, \mathcal{P}_{\text{out}}) = \Phi\left(\frac{\alpha}{\gamma} \cdot \frac{\sum_{i=1}^{N}(\boldsymbol{\theta}_i^T \boldsymbol{\mu})}{\|\sum_{i=1}^{N} \boldsymbol{\theta}_i\|\sigma} + \frac{\beta}{\gamma\sigma} \cdot \frac{\sum_{i=1}^{N}(\boldsymbol{\theta}_i^T \boldsymbol{\Delta})}{\|\sum_{i=1}^{N} \boldsymbol{\theta}_i\|}\right).$$

Substituting Eq.(20) and Eq.(21) into Eq.(19), we have

$$\mathcal{G}_{\text{avg}} \triangleq \frac{1}{N} \sum_{i=1}^{N} \mathcal{G}(g_i, \mathcal{P}_{\text{in}}, \mathcal{P}_{\text{out}}) = \frac{\beta}{\gamma\sigma} \cdot \frac{1}{N} \sum_{i=1}^{N} \frac{|\boldsymbol{\theta}_i^T \boldsymbol{\Delta}|}{\|\boldsymbol{\theta}_i\|},$$

$$\mathcal{G}_{\text{ens}} \triangleq \mathcal{G}(g_{\text{ens}}, \mathcal{P}_{\text{in}}, \mathcal{P}_{\text{out}}) = \frac{\beta}{\gamma\sigma} \cdot \frac{|\sum_{i=1}^{N}(\boldsymbol{\theta}_i^T \boldsymbol{\Delta})|}{\|\sum_{i=1}^{N} \boldsymbol{\theta}_i\|}. \tag{22}$$

If we are able to show that $\mathcal{G}_{\text{ens}} \leq \mathcal{G}_{\text{avg}}$ then the proof is finished. The derivations continue as follows.

$$\mathcal{G}_{\text{avg}} = \frac{\beta}{\gamma\sigma} \cdot \frac{1}{N} \sum_{i=1}^{N} \frac{\|\boldsymbol{\theta}_i\| \|\boldsymbol{\Delta}\| |\cos\langle \boldsymbol{\theta}_i, \boldsymbol{\Delta}\rangle|}{\|\boldsymbol{\theta}_i\|} = \frac{\beta}{\gamma\sigma} \cdot \|\boldsymbol{\Delta}\| \frac{|\cos\langle \boldsymbol{\theta}_1, \boldsymbol{\Delta}\rangle| + \cdots + |\cos\langle \boldsymbol{\theta}_N, \boldsymbol{\Delta}\rangle|}{N},$$

$$\mathcal{G}_{\text{ens}} = \frac{\beta}{\gamma\sigma} \cdot \frac{|\sum_{i=1}^{N}(\|\boldsymbol{\theta}_i\| \|\boldsymbol{\Delta}\| \cos\langle \boldsymbol{\theta}_i, \boldsymbol{\Delta}\rangle)|}{\|\sum_{i=1}^{N} \boldsymbol{\theta}_i\|} = \frac{\beta}{\gamma\sigma} \cdot \|\boldsymbol{\Delta}\| \left| \frac{\|\boldsymbol{\theta}_1\| \cos\langle \boldsymbol{\theta}_1, \boldsymbol{\Delta}\rangle + \cdots + \|\boldsymbol{\theta}_N\| \cos\langle \boldsymbol{\theta}_N, \boldsymbol{\Delta}\rangle}{\|\boldsymbol{\theta}_1 + \cdots + \boldsymbol{\theta}_N\|} \right|, \tag{23}$$

Now we make 2 assumptions:

1. The parameters $\boldsymbol{\theta}_i$ of these modes hold similar norms: $\|\boldsymbol{\theta}_1\| \approx \|\boldsymbol{\theta}_2\| \approx \cdots \approx \|\boldsymbol{\theta}_N\|$.

2. The parameters $\boldsymbol{\theta}_i$ of these modes are along one nearly consistent direction, *i.e.*, the angle between any 2 different parameters $\boldsymbol{\theta}_i$ and $\boldsymbol{\theta}_j$ is nearly 0.

Then,

$$\frac{\mathcal{G}_{\text{avg}}}{\mathcal{G}_{\text{ens}}} = \frac{|\cos\langle \boldsymbol{\theta}_1, \boldsymbol{\Delta}\rangle| + \cdots + |\cos\langle \boldsymbol{\theta}_N, \boldsymbol{\Delta}\rangle|}{|\|\boldsymbol{\theta}_1\| \cos\langle \boldsymbol{\theta}_1, \boldsymbol{\Delta}\rangle + \cdots + \|\boldsymbol{\theta}_N\| \cos\langle \boldsymbol{\theta}_N, \boldsymbol{\Delta}\rangle|} \cdot \frac{\|\boldsymbol{\theta}_1 + \cdots + \boldsymbol{\theta}_N\|}{N}$$

$$= \frac{|\cos\langle \boldsymbol{\theta}_1, \boldsymbol{\Delta}\rangle| + \cdots + |\cos\langle \boldsymbol{\theta}_N, \boldsymbol{\Delta}\rangle|}{|\cos\langle \boldsymbol{\theta}_1, \boldsymbol{\Delta}\rangle + \cdots + \cos\langle \boldsymbol{\theta}_N, \boldsymbol{\Delta}\rangle|} \geq 1. \tag{24}$$

The Proposition 1 is proved. □

Appendix D   Comprehensive empirical results

In this section, the comprehensive empirical results on OoD detection covering all the detectors, network structures and data sets are provided. The recognition results on the InD test data of all the modes trained on CIFAR10 and ImageNet-1K are shown in Sec.D.1. Section D.2 and Section D.3 illustrate the complete OoD detection results of each single mode and mode ensemble, respectively.

D.1   Classification accuracy on InD data

The classification accuracy of all the independent modes on their InD data sets CIFAR10 and ImageNet-1K is presented in Tab.13 and Tab.14, respectively. It is clearly shown that these isolated modes all hold consistently good recognition performance on their corresponding InD test sets.

network	capacity	mode-1	mode-2	mode-3	mode-4	mode-5	mode-6	mode-7	mode-8	mode-9	mode-10
RN18	11,173,962	93.21	93.33	93.61	93.26	93.68	93.57	93.60	93.85	93.79	93.91
WRN28X10	36,489,290	94.02	94.30	93.54	94.12	94.29	93.80	94.39	94.01	94.27	94.03

Table 13: The classification accuracy (%) of 10 isolated modes of 2 network structures, **RN18** and **WRN28X10**, on the **CIFAR10** test set as the InD data.

network	capacity	mode-1	mode-2	mode-3	mode-4	mode-5
RN50	25,557,032	74.84	74.71	74.86	74.65	74.80
DN121	7,978,856	74.25	74.30	74.46	74.29	74.33
T2T-ViT-14	21,545,550	81.30	81.44	81.53	-	-

Table 14: The classification accuracy (%) of 5 isolated modes of 2 network structures, **RN50** and **DN121**, and 3 isolated modes of **T2T-ViT-14**, on the **ImageNet-1K** validation set as the InD data.

D.2   OoD detection results of single modes

In this section, we provide the complete detection results on the OoD data sets of all single modes of different network structures trained on the CIFAR10 and ImageNet-1K benchmarks *w.r.t* different types of detectors.

Results on CIFAR10.   In Tab.15 and Tab.16, we record the detection performance of 10 isolated modes trained on CIFAR10 of ResNet18 and Wide ResNet28X10, respectively. The **best** and <u>worst</u> detection results are marked in the 2 tables for each mode on each OoD data set *w.r.t* 5 OoD detectors: MSP, ODIN, Energy, Mahalanobis and KNN.

As shown in Tab.15 and Tab.16, those isolated and independent modes clearly hold significantly varied OoD detection results on multiple OoD data sets for different types of OoD detectors. Taking the MSP method of ResNet18 as an example, the FPR values on the SVHN data set could range from the worst 77.76% to the best 65.20% with a 12.56% difference among the 10 modes. Besides, considering the mode-4 of ResNet18, ODIN achieves lower FPR values on SVHN (55.85%) than MSP (66.45%), while for mode-9, MSP (67.52%) instead outperforms ODIN (72.09%). The results of other OoD detectors on other OoD data sets all manifest such a common phenomenon, *i.e.*, a high variance on the OoD detection performance among the isolated and independent modes, which further indicates the high uncertainty of the detection performance on OoD data for single modes.

Results on ImageNet-1K.   In Tab.17 and Tab.18, we record the detection performance of 5 isolated modes trained from scratch on ImageNet-1K of ResNet50 and DenseNet121, respectively. The **best** and <u>worst</u> detection results are marked in the 2 tables for each mode on each OoD data set *w.r.t* 6 OoD detectors: MSP, ODIN, Energy, GradNorm, Mahalanobis and RankFeat.

As shown in Tab.17 and Tab.18, compared to the results on CIFAR10, those isolated and independent modes shows relatively more consistent detection performance. This might be due to that the training set size of ImageNet-1K (1,281,167) is much more larger than that of CIFAR10 (50,000), which benefits the model generalization both on InD data and OoD data as the model has "seen" much more numerous images during training. Nevertheless, the detection variances among those modes cannot be simply ignored, and the variance of DenseNet121 is larger and more evident than that of ResNet50, indicating that modes of different structures show different uncertainties. We reiterate

the 2 phenomena that reflect the high detection variances existed in the independent modes on both CIFAR10 and ImageNet-1K, which has been summarized in the manuscript:

- For a given OoD detection method, those independent modes hold significantly-fluctuating FPR results.

- For different modes, detection results among those detection methods can also be opposite. That is, detector A might outperform detector B on some mode, while detector B shows superiority over detector A on another mode.

D.3 OoD detection results of mode ensemble

In this section, we provide the complete detection results on the OoD data sets of ensembling multiple independent modes of different network structures on CIFAR10 and ImageNet-1K benchmarks *w.r.t* different types of detectors. The details of ensembling ways for each OoD detector have been elaborated in Appendix A of the main text.

Results on CIFAR10. For the 10 independent modes on CIFAR10, we ensemble $k \in \{1, 2, 4, 6, 8\}$ modes to verify the effectiveness of mode ensemble for OoD detection, shown in Tab.19 and Tab.20 for ResNet18 and Wide ResNet28X10, respectively. For $k = 1$, we report the average detection results of the total 10 modes with the mean values and standard deviations. For $k \in \{2, 4, 6, 8\}$, we randomly pick out k *different* modes from the 10 modes and perform mode ensemble, which is repeated 3 times, then the average detection results of the 3 random pickings are presented with the mean values and standard deviations.

As shown in Tab.19 and Tab.20, by ensembling multiple isolated modes, the variances of the detection results get reduced and the detection performance gets significantly improved. Taking the Mahalanobis method with ResNet18 as an example, its average detection FPR on SVHN of single modes is up to 24.66%, which is improved to 3.81% with a 20.85% reduction by ensembling 8 modes, while the variance simultaneously gets reduced from 12.72% to 0.52%.

Results on ImageNet-1K. For the 5 independent modes on ImageNet-1K, we ensemble $k \in \{1, 2, 3, 4\}$ modes to verify the effectiveness of mode ensemble for OoD detection, shown in Tab.21 and Tab.22 for ResNet50 and DenseNet121, respectively. For $k = 1$, we report the average detection results of the total 5 modes with the mean values and standard deviations. For $k \in \{2, 3, 4\}$, we randomly pick out k *different* modes from the 5 modes and perform mode ensemble, which is repeated 3 times, then the average detection results of the 3 random pickings are presented with the mean values and standard deviations.

As shown in Tab.21 and Tab.22, the mode ensemble could bring variance reduction and performance improvements for different OoD detectors. For example, considering the RankFeat method with DenseNet121, the average and the standard deviation of the detection FPR values on iNaturalist could be improved from 63.06% to 40.92% with a 22.14% reduction and from 13.98% to 5.41% with an 8.57% reduction, respectively.

In short, these detection results on both CIFAR10 and ImageNet-1K benchmarks with various OoD detectors and network structures have shown the 2 benefits brought by mode ensemble:

- For a given OoD detection method, its performance gets significantly improved via mode ensemble with both reduced variances and better detection results.

- Mode ensemble benefits the evaluation among different OoD detectors as it gets rid of the uncertainties of single modes.

Table 15: The detection performance of each mode of **ResNet18** trained on **CIFAR10** *w.r.t* 5 OoD detectors: MSP, ODIN, Energy, Mahalanobis and kNN. The **best** and **worst** results of each mode on each OoD data set are highlighted.

Modes	SVHN		LSUN		iSUN		Texture		Places365	
	FPR↓	AUROC↑	FPR↓	AUROC↑	FPR↓	AUROC↑	FPR↓	AUROC↑	FPR↓	AUROC↑
MSP										
mode-1	74.87	83.87	55.00	91.70	52.67	92.09	**67.36**	**87.26**	64.57	87.60
mode-2	71.58	86.86	53.19	92.07	**65.85**	88.92	65.07	88.25	65.23	87.76
mode-3	74.87	83.69	**56.30**	**90.94**	63.74	90.17	64.79	88.53	**65.61**	**87.46**
mode-4	66.45	89.15	50.01	92.52	61.85	90.21	65.66	88.63	64.97	87.84
mode-5	73.32	84.69	48.30	93.19	60.86	89.45	63.10	88.60	63.14	87.78
mode-6	**65.20**	89.09	51.25	92.44	59.88	90.84	**61.60**	**89.92**	63.56	87.89
mode-7	77.26	86.00	50.81	92.50	65.21	**88.74**	63.21	88.31	63.53	87.55
mode-8	**77.76**	**83.30**	51.12	92.57	**49.45**	**93.02**	63.63	88.64	63.32	87.88
mode-9	67.52	88.83	51.82	92.92	60.04	90.82	64.06	88.79	64.69	87.68
mode-10	68.01	**89.65**	**43.08**	**94.07**	58.68	90.86	63.39	88.88	**62.83**	**88.30**
ODIN										
mode-1	72.98	81.82	26.70	95.39	23.53	96.00	**62.57**	**85.74**	48.04	89.34
mode-2	71.33	84.87	25.16	95.58	**44.21**	92.46	60.07	86.45	48.93	89.11
mode-3	76.52	**79.16**	**29.63**	**94.30**	34.76	94.39	54.88	87.94	**50.48**	**88.42**
mode-4	**55.85**	**88.81**	22.09	95.73	37.85	93.32	55.46	87.91	47.74	88.95
mode-5	67.92	85.33	18.83	96.85	41.10	**91.95**	54.91	87.93	49.03	88.89
mode-6	59.50	88.21	21.29	96.18	35.20	93.81	**48.12**	**90.27**	**45.59**	89.45
mode-7	72.02	83.45	21.28	96.22	39.91	93.54	56.08	86.98	48.89	88.52
mode-8	**82.60**	79.29	25.15	95.77	**23.19**	**96.02**	56.76	87.82	48.49	89.18
mode-9	72.09	84.64	20.23	96.36	37.41	93.80	56.21	87.02	48.04	88.84
mode-10	67.90	88.65	**14.53**	**97.38**	32.59	94.64	54.77	88.15	46.09	**90.00**
Energy										
mode-1	74.86	81.63	28.78	95.09	**26.66**	95.52	**63.67**	**85.87**	47.89	89.49
mode-2	75.22	84.76	27.84	95.33	**48.77**	91.66	62.07	86.67	49.45	89.32
mode-3	78.63	79.66	**30.99**	**94.19**	39.16	93.66	55.05	88.27	**50.34**	**88.65**
mode-4	**59.05**	**89.01**	24.01	95.62	43.03	92.66	57.71	88.06	48.81	89.15
mode-5	70.56	85.11	21.06	96.57	44.22	**91.24**	55.92	88.10	48.84	89.12
mode-6	62.67	88.40	22.73	96.02	39.92	92.96	**49.54**	**90.37**	**45.73**	89.64
mode-7	72.61	84.10	22.03	96.12	43.70	92.61	56.49	87.42	48.55	88.84
mode-8	**84.44**	**79.21**	27.99	95.51	27.46	**95.54**	57.91	88.01	49.23	89.32
mode-9	75.91	84.69	22.33	96.23	42.75	93.06	57.91	87.44	48.62	89.09
mode-10	71.11	88.51	**15.04**	**97.32**	35.31	94.09	55.27	88.49	46.33	**90.10**
Mahalanobis										
mode-1	38.26	89.52	68.10	78.51	15.05	93.92	**69.15**	**57.90**	**92.69**	**59.35**
mode-2	**45.30**	89.92	75.27	75.85	64.41	75.46	38.79	87.48	92.39	65.74
mode-3	11.22	97.21	75.15	60.15	10.32	97.21	27.94	89.78	87.71	62.28
mode-4	25.49	92.30	75.58	79.01	8.89	97.87	51.21	74.12	86.43	69.90
mode-5	15.48	96.31	**84.38**	**54.03**	**85.47**	**44.85**	31.72	87.74	89.92	62.33
mode-6	40.42	**88.16**	79.89	69.72	**4.53**	**98.62**	59.96	67.98	89.56	65.15
mode-7	25.64	93.61	72.10	78.23	30.16	88.87	58.30	70.00	**82.43**	**72.59**
mode-8	**10.40**	**97.54**	67.36	77.06	8.32	97.82	36.19	86.61	91.67	61.73
mode-9	20.13	94.30	73.10	**79.27**	13.13	95.93	42.39	80.21	84.74	69.65
mode-10	14.29	96.68	82.36	63.37	13.78	97.18	**22.18**	**94.04**	87.33	67.13
kNN										
mode-1	44.24	93.56	39.55	94.08	33.92	94.41	42.96	92.42	53.70	**88.31**
mode-2	48.67	92.34	40.68	93.45	42.04	92.91	**45.59**	**92.15**	52.67	89.07
mode-3	48.96	92.23	38.15	93.80	38.66	93.58	41.37	92.74	52.82	88.74
mode-4	50.08	92.34	41.41	93.33	37.71	93.73	45.55	92.35	**53.86**	89.07
mode-5	62.06	89.79	38.08	94.16	39.75	93.25	41.26	92.95	52.10	**89.08**
mode-6	41.03	93.48	**50.43**	**92.37**	37.08	93.84	41.86	93.02	53.13	88.93

Table 15 – continued from previous page

Modes	OoD data sets									
	SVHN		LSUN		iSUN		Texture		Places365	
	FPR↓	AUROC↑	FPR↓	AUROC↑	FPR↓	AUROC↑	FPR↓	AUROC↑	FPR↓	AUROC↑
mode-7	**71.17**	**89.38**	42.01	93.49	**45.18**	**92.24**	42.73	92.80	53.37	88.71
mode-8	66.00	90.28	41.60	93.92	**31.11**	**95.12**	44.91	92.67	53.02	88.94
mode-9	38.29	94.33	36.58	94.49	40.45	93.54	**39.26**	**93.37**	53.64	88.76
mode-10	**36.87**	**94.43**	**32.10**	**94.96**	38.49	93.46	40.44	92.86	**51.84**	88.90

Table 16: The detection performance of each mode of **Wide ResNet28X10** trained on **CIFAR10** *w.r.t* 5 OoD detectors: MSP, ODIN, Energy, Mahalanobis and kNN. The **best** and **worst** results of each mode are highlighted.

Modes	OoD data sets									
	SVHN		LSUN		iSUN		Texture		Places365	
	FPR↓	AUROC↑	FPR↓	AUROC↑	FPR↓	AUROC↑	FPR↓	AUROC↑	FPR↓	AUROC↑
MSP										
mode-1	54.52	93.54	**32.95**	**95.66**	46.82	93.59	60.90	89.12	62.48	88.44
mode-2	**30.10**	95.62	27.41	96.29	52.13	92.71	**64.04**	88.08	**57.17**	**89.84**
mode-3	45.38	94.01	23.21	96.57	47.41	93.58	53.65	90.95	**62.54**	**88.12**
mode-4	**60.18**	**91.23**	32.71	95.80	52.25	92.83	62.27	89.82	62.00	88.22
mode-5	43.60	94.00	26.34	96.25	52.25	92.77	60.55	89.30	59.62	89.06
mode-6	37.53	94.38	**17.96**	**97.26**	40.64	94.23	**48.32**	**91.76**	59.19	88.83
mode-7	53.86	92.12	27.23	96.13	**40.19**	**94.46**	60.30	**88.03**	57.34	89.55
mode-8	44.99	94.24	21.92	96.85	**66.53**	**89.79**	62.45	88.59	57.71	89.76
mode-9	46.18	93.92	24.57	96.37	42.10	93.92	53.65	91.36	60.16	88.85
mode-10	31.58	**95.65**	28.90	95.97	49.74	93.22	57.38	90.50	59.94	88.64
ODIN										
mode-1	24.29	96.09	6.86	98.71	21.27	96.40	48.85	89.21	47.49	89.76
mode-2	16.52	96.93	6.00	98.87	25.88	96.07	**54.10**	**88.20**	38.79	92.22
mode-3	20.24	96.46	5.37	98.93	19.71	96.66	37.52	92.30	**50.40**	**89.25**
mode-4	44.97	92.36	6.26	98.76	30.67	94.94	52.73	88.95	49.23	88.77
mode-5	23.83	96.05	5.26	98.94	24.27	96.01	50.32	89.01	46.48	90.08
mode-6	22.12	96.40	**3.50**	**99.28**	21.56	96.45	**37.09**	**92.40**	46.72	90.26
mode-7	**45.82**	**92.34**	5.45	98.85	19.61	96.44	52.73	86.02	39.11	91.36
mode-8	20.86	96.54	3.63	99.24	**36.62**	**94.38**	52.30	88.72	**38.53**	**92.16**
mode-9	25.96	95.85	5.36	98.87	**16.96**	**96.81**	39.18	92.32	43.67	90.67
mode-10	**13.69**	**97.61**	**7.46**	**98.68**	27.27	95.63	45.16	90.95	46.06	89.97
Energy										
mode-1	24.22	96.09	7.44	**98.60**	25.33	95.77	49.88	89.03	47.43	89.83
mode-2	15.78	97.05	6.20	98.83	32.44	95.15	**55.51**	**88.01**	38.80	**92.22**
mode-3	18.99	96.66	6.08	98.85	23.92	96.03	39.49	91.97	**50.79**	89.25
mode-4	42.75	92.76	6.56	98.69	37.20	94.04	53.76	88.87	49.48	**88.92**
mode-5	23.37	96.07	5.92	98.84	28.71	95.37	51.24	88.95	46.71	90.17
mode-6	21.94	96.38	**3.85**	**99.21**	25.64	95.86	**38.51**	92.12	47.43	90.18
mode-7	**48.05**	**92.23**	5.85	98.77	24.86	**96.58**	55.21	86.00	39.19	91.44
mode-8	20.87	96.57	3.96	99.19	**43.41**	**93.37**	54.26	88.41	**38.55**	**92.22**
mode-9	25.18	96.02	6.32	98.78	**20.65**	96.31	40.51	**92.17**	44.65	90.65
mode-10	**12.43**	**97.74**	**7.48**	98.65	34.35	94.67	47.18	90.58	45.87	90.10
Mahalanobis										
mode-1	3.91	99.09	**63.06**	**82.65**	5.47	98.65	**16.77**	**95.07**	**81.80**	**72.57**
mode-2	6.94	98.46	79.02	74.97	5.93	98.65	24.36	93.41	86.63	68.60
mode-3	10.93	97.44	77.92	76.55	9.28	97.67	28.99	91.06	86.27	66.88
mode-4	**2.94**	**99.20**	67.43	78.59	6.23	98.39	17.73	94.48	82.10	72.09
mode-5	5.69	98.68	67.35	81.57	5.46	98.63	22.73	93.21	84.45	70.65
mode-6	**64.41**	**86.19**	**90.87**	**65.72**	**10.91**	**96.79**	**46.19**	**83.97**	**89.61**	**65.51**
mode-7	6.81	98.55	78.26	76.43	6.31	98.40	24.59	92.87	85.76	69.93

Table 16 – continued from previous page

Modes	SVHN		LSUN		iSUN		Texture		Places365	
					OoD data sets					
	FPR↓	AUROC↑	FPR↓	AUROC↑	FPR↓	AUROC↑	FPR↓	AUROC↑	FPR↓	AUROC↑
mode-8	4.36	98.93	70.49	77.11	6.83	98.37	18.03	94.39	83.65	70.72
mode-9	7.86	98.09	73.04	76.48	6.32	98.36	22.89	93.34	85.01	68.50
mode-10	6.80	98.37	71.34	78.83	**4.95**	**98.71**	23.09	92.81	85.54	69.15
					kNN					
mode-1	**30.51**	**95.48**	21.47	96.45	21.94	96.34	36.21	94.21	47.06	90.22
mode-2	17.35	97.22	21.79	96.52	28.21	95.47	42.64	92.79	43.30	91.28
mode-3	22.78	96.58	18.43	96.90	26.95	95.74	30.60	95.16	**50.97**	**89.44**
mode-4	25.12	96.25	**23.10**	**96.36**	32.10	94.92	37.71	94.07	47.83	89.97
mode-5	25.78	96.27	21.75	96.58	32.06	95.01	35.76	94.19	45.94	90.73
mode-6	22.78	96.36	**15.21**	**97.50**	21.50	96.39	**28.51**	**95.29**	48.39	89.59
mode-7	30.43	95.51	19.72	96.87	**18.17**	**96.91**	40.94	93.67	**42.11**	**91.48**
mode-8	19.10	96.94	19.41	96.87	**42.07**	**92.89**	**45.20**	**92.38**	42.51	91.43
mode-9	22.45	96.58	19.18	97.00	26.43	95.73	31.84	94.84	50.16	89.90
mode-10	**17.18**	**97.37**	22.28	96.35	19.31	96.78	31.31	94.93	46.00	90.39

Modes	OoD data sets							
	iNaturalist		SUN		Places		Texture	
	FPR↓	AUROC↑	FPR↓	AUROC↑	FPR↓	AUROC↑	FPR↓	AUROC↑
MSP								
mode-1	57.33	87.29	70.84	**80.65**	72.49	**80.44**	67.20	**81.10**
mode-2	**55.43**	**87.95**	70.50	**81.35**	72.82	80.43	**69.54**	79.88
mode-3	55.84	87.89	**70.06**	81.11	72.63	80.31	**65.89**	81.04
mode-4	55.95	87.49	70.81	80.70	**72.96**	**80.15**	68.33	**79.84**
mode-5	**59.73**	**86.87**	**71.55**	80.80	**72.34**	80.29	69.08	80.38
ODIN								
mode-1	53.69	90.15	60.23	86.32	63.79	84.89	55.34	86.40
mode-2	**52.80**	**90.31**	59.09	**87.05**	**62.72**	**85.07**	**57.62**	85.39
mode-3	53.01	90.28	**58.66**	86.80	63.78	84.73	**53.39**	**86.50**
mode-4	54.39	89.90	60.11	85.99	**64.90**	**84.33**	57.27	**85.00**
mode-5	**56.56**	**89.55**	**60.28**	86.17	63.45	84.68	56.12	85.76
Energy								
mode-1	56.13	89.61	58.21	86.63	62.27	84.99	53.78	86.61
mode-2	**56.06**	**89.64**	56.88	**87.37**	**61.85**	**85.21**	55.53	85.63
mode-3	56.35	89.54	**56.44**	87.08	62.50	84.80	**51.44**	**86.76**
mode-4	57.70	89.22	58.62	**86.23**	**63.58**	**84.36**	**55.67**	**85.19**
mode-5	**59.45**	**88.90**	**58.75**	86.42	62.62	84.78	54.49	85.98
GradNorm								
mode-1	57.90	83.27	63.94	79.64	71.55	75.51	59.72	79.85
mode-2	53.97	85.28	63.82	80.08	72.09	75.86	**62.39**	78.32
mode-3	**52.03**	**85.71**	**61.13**	**80.78**	**70.67**	**76.26**	**55.05**	**81.10**
mode-4	57.42	83.62	64.47	78.40	73.30	74.34	61.01	**78.18**
mode-5	**63.03**	**81.45**	**67.78**	**78.02**	**74.47**	**74.43**	61.95	78.79
Mahalanobis								
mode-1	96.66	54.33	**97.38**	49.83	**96.95**	**50.44**	36.79	85.52
mode-2	**95.04**	**59.89**	**96.35**	**53.62**	**96.05**	51.92	**33.87**	**88.19**
mode-3	97.06	48.77	96.63	50.74	96.23	52.32	45.90	74.52
mode-4	97.35	48.14	96.85	50.56	96.10	**53.33**	44.80	75.80
mode-5	**97.58**	**46.06**	96.99	**48.11**	96.12	51.20	**53.74**	**67.49**
RankFeat								
mode-1	83.89	71.16	79.96	76.63	83.18	72.18	55.05	85.81
mode-2	78.78	**72.18**	80.51	76.56	85.82	71.56	65.78	78.05
mode-3	**95.46**	**46.77**	80.17	76.74	84.16	71.89	**72.94**	**73.83**
mode-4	94.02	55.37	**94.02**	**59.55**	**94.49**	**56.68**	71.67	76.61
mode-5	**78.26**	70.35	**76.58**	**77.42**	**81.29**	**72.41**	**53.71**	**85.48**

Table 17: The detection performance of each of the 5 modes of **ResNet50** trained from scratch on **ImageNet-1K** *w.r.t* 6 OoD detectors: MSP, ODIN, Energy, GradNorm, Mahalanobis and RankFeat. The **best** and **worst** results of each mode on each OoD data set are highlighted.

Modes	OoD data sets							
	iNaturalist		SUN		Places		Texture	
	FPR↓	AUROC↑	FPR↓	AUROC↑	FPR↓	AUROC↑	FPR↓	AUROC↑
MSP								
mode-1	58.44	87.18	**<u>71.11</u>**	80.78	**<u>74.11</u>**	**<u>79.69</u>**	67.07	80.72
mode-2	**<u>55.68</u>**	**<u>87.28</u>**	**<u>68.78</u>**	**<u>81.49</u>**	**<u>70.85</u>**	**<u>80.63</u>**	66.21	**<u>80.27</u>**
mode-3	58.29	87.10	70.60	81.02	73.01	80.07	66.06	80.70
mode-4	58.52	87.20	70.73	80.81	72.79	79.77	**<u>67.85</u>**	80.46
mode-5	**<u>60.97</u>**	**<u>86.19</u>**	70.82	**<u>80.69</u>**	72.76	79.89	**<u>64.41</u>**	**<u>80.93</u>**
ODIN								
mode-1	54.88	89.39	**<u>60.26</u>**	**<u>85.76</u>**	**<u>65.84</u>**	**<u>83.33</u>**	54.36	86.61
mode-2	**<u>50.56</u>**	90.21	**<u>55.79</u>**	**<u>87.00</u>**	**<u>60.81</u>**	**<u>85.08</u>**	53.35	**<u>86.62</u>**
mode-3	51.61	90.12	57.90	86.08	63.82	**<u>85.08</u>**	53.35	**<u>86.62</u>**
mode-4	51.47	**<u>90.26</u>**	59.03	86.28	63.56	84.01	**<u>55.12</u>**	86.20
mode-5	**<u>58.13</u>**	**<u>88.39</u>**	59.17	85.84	63.17	84.07	**<u>51.83</u>**	**<u>86.19</u>**
Energy								
mode-1	56.24	88.63	**<u>57.85</u>**	**<u>85.99</u>**	**<u>64.35</u>**	**<u>83.29</u>**	51.93	86.98
mode-2	**<u>52.86</u>**	89.67	**<u>53.31</u>**	**<u>87.32</u>**	**<u>59.77</u>**	**<u>85.16</u>**	50.76	**<u>87.05</u>**
mode-3	53.19	89.61	55.89	86.35	62.05	84.13	50.64	86.86
mode-4	53.31	**<u>89.77</u>**	56.85	86.58	62.75	84.08	**<u>53.56</u>**	86.53
mode-5	**<u>60.92</u>**	**<u>87.56</u>**	56.76	86.07	61.93	84.11	**<u>49.93</u>**	**<u>86.46</u>**
GradNorm								
mode-1	73.79	77.93	72.64	75.03	**<u>81.21</u>**	70.23	66.15	77.82
mode-2	69.99	79.89	**<u>68.30</u>**	76.72	**<u>75.71</u>**	72.63	**<u>63.30</u>**	**<u>78.74</u>**
mode-3	69.93	79.67	69.12	**<u>77.56</u>**	77.22	**<u>73.34</u>**	64.06	78.48
mode-4	**<u>66.85</u>**	**<u>81.07</u>**	72.51	75.61	80.08	71.44	65.87	77.27
mode-5	**<u>77.07</u>**	**<u>73.47</u>**	**<u>73.66</u>**	**<u>73.88</u>**	80.59	**<u>69.90</u>**	**<u>66.83</u>**	**<u>76.39</u>**
Mahalanobis								
mode-1	89.20	63.79	84.50	**<u>70.98</u>**	83.84	71.65	**<u>43.56</u>**	**<u>75.46</u>**
mode-2	**<u>93.31</u>**	60.90	85.98	68.14	83.87	71.11	**<u>65.21</u>**	**<u>58.26</u>**
mode-3	**<u>88.43</u>**	**<u>69.11</u>**	86.21	70.74	85.17	72.50	51.40	70.16
mode-4	91.84	**<u>58.88</u>**	**<u>86.82</u>**	**<u>66.23</u>**	**<u>85.54</u>**	69.64	49.86	68.64
mode-5	92.43	59.27	**<u>82.07</u>**	70.24	**<u>81.02</u>**	**<u>72.95</u>**	57.20	63.21
RankFeat								
mode-1	66.01	85.91	**<u>75.53</u>**	**<u>80.27</u>**	**<u>79.95</u>**	**<u>75.64</u>**	43.60	**<u>90.35</u>**
mode-2	58.49	83.77	**<u>34.70</u>**	**<u>92.02</u>**	**<u>50.70</u>**	**<u>86.12</u>**	32.73	92.45
mode-3	59.53	85.17	50.07	88.37	63.27	82.05	40.64	91.54
mode-4	**<u>84.70</u>**	**<u>78.61</u>**	69.57	83.82	76.45	78.21	**<u>49.89</u>**	90.81
mode-5	**<u>46.58</u>**	**<u>87.27</u>**	44.46	88.42	58.95	81.54	**<u>22.48</u>**	**<u>94.15</u>**

Table 18: The detection performance of each of the 5 modes of **DenseNet121** trained from scratch on **ImageNet-1K** *w.r.t* 6 OoD detectors: MSP, ODIN, Energy, GradNorm, Mahalanobis and RankFeat. The **<u>best</u>** and **<u>worst</u>** results of each mode on each OoD data set are highlighted.

Ensemble of k modes	SVHN FPR↓	SVHN AUROC↑	LSUN FPR↓	LSUN AUROC↑	iSUN FPR↓	iSUN AUROC↑	Texture FPR↓	Texture AUROC↑	Places365 FPR↓	Places365 AUROC↑
MSP										
$k=1$	71.68±4.61	86.51±2.53	51.09±3.66	92.49±0.84	59.82±5.23	90.51±1.34	64.19±1.60	88.58±0.66	64.15±0.98	87.77±0.23
$k=2$	68.23±5.74	88.46±1.84	43.56±6.07	93.75±0.71	51.71±4.49	92.68±0.89	58.54±2.26	90.35±0.35	59.35±1.15	89.10±0.14
$k=4$	66.34±5.25	88.95±2.60	44.98±3.70	93.66±0.63	55.71±2.39	91.88±0.54	57.69±0.47	90.79±0.33	58.87±0.57	89.49±0.14
$k=6$	**67.03±0.91**	**89.34±0.68**	**44.99±1.40**	**93.82±0.21**	55.04±2.61	92.31±0.76	**57.49±0.35**	**91.03±0.09**	**58.75±0.37**	**89.73±0.05**
$k=8$	66.70±1.67	89.22±0.70	44.56±1.65	93.83±0.24	**54.02±0.85**	**92.40±0.14**	56.87±0.78	91.16±0.14	57.88±0.47	89.81±0.05
ODIN										
$k=1$	69.87±7.74	84.42±3.56	22.49±4.32	95.98±0.84	34.98±6.97	93.99±1.33	55.98±3.75	87.62±1.22	48.13±1.43	89.07±0.46
$k=2$	69.90±6.36	86.50±2.66	21.59±4.37	96.35±0.78	33.04±10.60	95.05±1.42	51.58±2.43	90.05±0.43	46.14±1.55	90.34±0.50
$k=4$	64.13±3.16	89.11±1.20	18.64±2.99	96.85±0.42	25.56±2.15	**96.16±0.23**	46.09±1.72	91.51±0.34	42.53±1.53	91.06±0.24
$k=6$	**59.88±0.40**	**90.15±0.15**	17.50±0.85	96.99±0.12	28.21±2.05	95.86±0.29	44.82±0.65	91.73±0.12	**40.85±0.11**	**91.44±0.03**
$k=8$	61.74±2.23	89.71±0.39	**17.16±0.66**	**97.09±0.12**	27.00±2.58	96.05±0.32	**44.61±0.34**	**91.86±0.05**	40.58±0.16	91.57±0.04
Energy										
$k=1$	72.51±7.36	84.51±3.53	24.28±4.70	95.80±0.86	39.10±7.26	93.30±1.44	57.15±3.89	87.87±1.19	48.38±1.40	89.27±0.41
$k=2$	64.19±6.50	88.93±1.67	18.41±3.26	96.83±0.47	31.12±6.61	94.71±1.30	48.51±2.63	90.79±0.41	42.97±0.96	90.76±0.19
$k=4$	67.45±5.59	88.20±1.32	18.83±1.87	96.83±0.33	25.86±6.93	95.97±1.04	47.01±2.15	91.44±0.43	40.96±0.57	91.41±0.25
$k=6$	63.39±1.43	89.58±0.46	17.65±1.11	97.01±0.16	29.10±0.82	95.66±0.17	45.19±0.65	**91.85±0.08**	40.39±0.41	91.51±0.08
$k=8$	**64.21±0.90**	**89.67±0.42**	**16.55±0.08**	**97.19±0.05**	**26.17±0.75**	**96.09±0.07**	45.24±0.60	91.84±0.11	**39.73±0.19**	**91.72±0.08**
Mahalanobis										
$k=1$	24.66±12.72	93.56±3.45	75.33±5.61	71.52±9.22	25.41±27.43	88.77±16.96	43.78±15.34	79.59±11.63	88.49±3.39	65.59±4.24
$k=2$	11.17±5.53	97.20±1.40	73.92±16.15	73.54±11.02	45.01±36.43	73.58±29.89	44.41±12.95	79.48±8.28	87.60±2.22	69.09±4.01
$k=4$	4.68±1.28	98.88±0.26	75.31±6.14	75.88±2.82	20.38±9.28	93.71±3.42	**27.71±2.11**	**91.25±0.82**	85.58±1.83	73.72±2.28
$k=6$	5.24±2.23	98.71±0.49	**70.82±0.70**	**78.01±1.98**	28.25±21.42	86.76±11.95	31.24±8.38	88.04±5.04	83.62±1.58	74.41±1.41
$k=8$	**3.81±0.52**	**99.08±0.17**	77.27±1.89	76.59±2.20	**11.62±5.34**	**95.91±3.04**	25.44±8.76	91.85±3.95	**82.11±0.93**	**77.09±0.06**
kNN										
$k=1$	50.74±11.88	92.22±1.84	40.06±4.70	93.81±0.71	38.44±3.95	93.61±0.78	42.59±2.18	92.73±0.36	53.02±0.67	88.85±0.24
$k=2$	47.14±5.67	93.19±0.26	45.19±6.06	93.17±1.02	29.78±5.46	95.43±0.75	38.42±2.04	93.79±0.29	52.82±1.31	89.36±0.14
$k=4$	48.63±6.45	92.96±1.00	52.19±1.92	**91.90±0.25**	31.54±2.97	95.31±0.44	35.53±1.14	94.32±0.14	53.82±1.30	89.36±0.06
$k=6$	47.35±1.55	93.41±0.34	54.81±2.41	91.58±0.57	27.49±2.09	95.89±0.21	33.82±0.47	94.64±0.12	54.70±0.29	89.40±0.12
$k=8$	**47.34±0.74**	**93.32±0.17**	**57.44±0.91**	91.05±0.31	**28.98±0.98**	**95.82±0.09**	**35.22±0.17**	**94.52±0.05**	**56.34±0.26**	**89.24±0.07**

Table 19: The detection performance of ensembling k modes (**ResNet18** trained on **CIFAR10**) on each OoD data set *w.r.t* different types of OoD detectors. The results with the **lowest variances** are highlighted with bold fonts.

Ensemble of k modes	SVHN FPR↓	SVHN AUROC↑	LSUN FPR↓	LSUN AUROC↑	iSUN FPR↓	iSUN AUROC↑	Texture FPR↓	Texture AUROC↑	Places365 FPR↓	Places365 AUROC↑
MSP										
$k=1$	44.79±9.78	93.87±1.37	26.32±4.66	96.32±0.48	49.01±7.75	93.11±1.32	58.35±5.00	89.75±1.35	59.82±2.04	88.93±0.62
$k=2$	33.72±4.01	95.36±0.42	20.88±1.48	96.92±0.13	45.66±5.05	93.92±0.74	54.54±2.22	90.77±0.74	55.88±1.58	89.99±0.40
$k=4$	**35.16±1.04**	95.17±0.30	18.68±1.53	**97.11±0.08**	36.86±2.28	**95.13±0.16**	**52.10±1.14**	91.43±0.41	54.04±1.46	90.50±0.21
$k=6$	36.91±2.24	95.23±0.24	20.10±1.15	97.04±0.16	40.51±5.81	94.88±0.62	53.21±2.89	91.65±0.56	**55.11±0.42**	**90.50±0.03**
$k=8$	34.02±2.53	**95.51±0.21**	**19.96±1.12**	97.03±0.13	39.96±2.29	94.97±0.21	54.11±1.44	**91.46±0.24**	54.16±0.89	90.73±0.13
ODIN										
$k=1$	25.83±10.93	95.66±1.82	5.52±1.25	98.91±0.20	24.38±5.94	95.98±0.78	47.00±6.76	89.81±2.12	44.65±4.41	90.45±1.16
$k=2$	20.99±8.56	96.64±1.12	3.94±0.64	99.12±0.15	15.92±1.78	97.26±0.30	39.39±4.93	92.31±1.24	41.12±3.02	91.57±0.69
$k=4$	17.33±3.30	97.06±0.36	3.61±0.39	99.13±0.05	16.66±3.58	97.15±0.42	39.32±3.70	92.45±0.82	39.52±2.13	91.83±0.44
$k=6$	16.01±2.08	97.22±0.24	3.29±0.11	99.18±0.03	14.49±1.34	97.41±0.11	40.60±4.31	91.92±1.03	37.15±1.25	92.38±0.43
$k=8$	**14.29±0.38**	**97.48±0.09**	**3.02±0.04**	**99.24±0.01**	**12.79±0.55**	**97.62±0.06**	**38.48±1.59**	**92.52±0.33**	**36.91±0.23**	**92.50±0.04**
Energy										
$k=1$	25.36±11.32	95.76±1.80	5.97±1.23	98.84±0.21	29.65±7.06	95.32±1.03	48.56±6.76	89.61±2.05	44.89±4.51	90.50±1.14
$k=2$	21.86±5.03	96.39±0.67	4.52±0.82	99.04±0.13	20.28±7.02	96.59±0.85	41.99±3.83	91.55±0.82	41.42±3.51	91.27±0.79
$k=4$	**11.21±1.10**	**97.88±0.06**	3.24±0.31	99.28±0.06	16.97±1.20	97.14±0.12	39.32±2.29	92.40±0.47	37.06±2.04	92.55±0.34
$k=6$	15.28±2.01	97.28±0.28	2.96±0.39	99.29±0.07	15.07±0.54	97.30±0.08	**39.31±0.72**	92.24±0.25	36.86±0.85	**92.39±0.15**
$k=8$	13.78±1.56	97.51±0.23	**2.76±0.06**	**99.31±0.04**	**13.25±0.12**	**97.53±0.03**	38.33±0.90	**92.42±0.12**	36.09±0.77	92.61±0.23
Mahalanobis										
$k=1$	12.07±18.53	97.30±3.94	73.88±7.96	76.89±4.60	6.77±1.87	98.26±0.60	24.54±8.47	92.46±3.18	85.08±2.29	69.46±2.21
$k=2$	11.26±9.37	97.69±1.56	76.36±7.70	76.37±4.10	6.97±1.54	98.18±0.47	22.90±5.43	93.48±1.46	85.61±1.99	70.02±2.12
$k=4$	5.24±1.46	98.80±0.32	75.79±1.29	76.04±1.23	5.39±0.99	98.66±0.27	**18.68±0.70**	**94.93±0.04**	80.39±1.18	75.05±0.85
$k=6$	7.09±1.64	98.42±0.32	80.74±4.29	69.44±3.00	6.40±1.63	98.35±0.46	20.44±2.89	94.03±1.18	79.64±1.26	**75.43±0.77**
$k=8$	**5.09±1.18**	**98.85±0.26**	82.97±1.25	68.46±1.04	**5.56±0.55**	**98.67±0.18**	16.68±0.93	95.69±0.49	**78.05±0.49**	77.98±0.82
kNN										
$k=1$	23.35±4.76	96.46±0.63	20.23±2.34	96.74±0.36	26.87±7.25	95.62±1.18	36.07±5.58	94.15±0.98	46.43±3.07	90.44±0.76
$k=2$	17.39±1.30	97.36±0.17	16.36±0.99	97.35±0.20	21.23±6.68	96.67±0.90	29.37±4.27	95.48±0.65	43.91±1.73	91.20±0.37
$k=4$	16.61±1.50	97.56±0.19	**14.67±0.07**	**97.74±0.02**	14.48±0.72	**97.60±0.06**	26.00±1.64	96.05±0.19	43.44±2.23	91.53±0.38
$k=6$	13.93±0.39	**97.94±0.04**	14.34±0.47	97.87±0.06	13.00±1.55	97.90±0.17	23.70±0.62	96.50±0.06	43.60±1.30	91.67±0.17
$k=8$	**13.57±0.34**	98.04±0.07	13.74±0.19	97.97±0.04	**12.71±0.49**	97.96±0.09	**23.48±0.09**	**96.58±0.02**	43.87±1.13	91.75±0.16

Table 20: The detection performance of ensembling k modes (**Wide ResNet28X10** trained on **CIFAR10**) on each OoD data set *w.r.t* different types of OoD detectors. The results with the **lowest variances** are highlighted with bold fonts.

Ensemble of k modes	OoD data sets							
	iNaturalist		SUN		Places		Textures	
	FPR↓	AUROC↑	FPR↓	AUROC↑	FPR↓	AUROC↑	FPR↓	AUROC↑
MSP								
$k=1$	56.86±1.76	87.50±0.45	70.75±0.55	80.92±0.30	72.65±0.25	80.32±0.12	68.01±1.48	80.45±0.61
$k=2$	53.08±1.10	88.64±0.29	69.41±0.39	81.71±0.12	70.79±0.22	81.18±0.11	65.46±0.63	81.44±0.26
$k=3$	52.22±0.68	88.98±0.21	69.09±0.33	82.00±0.09	**70.74±0.18**	81.42±0.03	64.74±1.26	81.82±0.39
$k=4$	**51.78±0.55**	**89.09±0.06**	**69.02±0.10**	**82.08±0.07**	70.24±0.24	**81.58±0.02**	**63.70±0.66**	**82.10±0.20**
ODIN								
$k=1$	54.09±1.52	90.04±0.32	59.67±0.75	86.47±0.44	63.73±0.79	84.74±0.28	55.95±1.69	85.81±0.64
$k=2$	50.17±0.63	91.44±0.16	57.59±0.37	87.53±0.07	61.73±0.36	85.87±0.09	51.64±1.32	87.81±0.37
$k=3$	48.96±0.84	91.79±0.08	**57.15±0.21**	87.64±0.20	61.11±0.12	**86.04±0.05**	49.95±0.98	88.24±0.31
$k=4$	**47.72±0.57**	**92.03±0.05**	56.48±0.33	**87.91±0.03**	**60.75±0.09**	86.25±0.06	**49.37±0.35**	**88.50±0.18**
Energy								
$k=1$	57.14±1.45	89.38±0.32	57.78±1.05	86.75±0.47	62.56±0.64	84.83±0.31	54.18±1.72	86.03±0.66
$k=2$	53.40±0.80	90.86±0.20	55.46±0.59	87.57±0.24	**60.02±0.07**	85.82±0.12	48.66±0.88	88.07±0.50
$k=3$	52.00±0.67	91.34±0.07	**54.02±0.18**	88.18±0.13	59.44±0.25	**86.38±0.06**	46.81±0.56	88.92±0.15
$k=4$	**51.75±0.24**	**91.51±0.04**	53.93±0.27	**88.26±0.13**	59.20±0.15	86.44±0.09	**46.09±0.48**	**89.03±0.18**
GradNorm								
$k=1$	56.87±4.22	83.87±1.71	64.23±2.37	79.38±1.15	72.42±1.49	75.28±0.86	60.02±2.96	79.25±1.23
$k=2$	52.67±1.41	86.14±0.48	61.02±1.14	81.14±0.52	69.99±0.99	77.02±0.40	56.49±2.46	81.67±1.20
$k=3$	53.24±1.57	86.16±0.59	61.28±0.93	81.25±0.42	69.85±0.52	77.27±0.31	56.82±1.16	82.11±0.62
$k=4$	**50.73±0.80**	**87.15±0.27**	**60.08±0.54**	**81.89±0.20**	**69.02±0.40**	**77.83±0.15**	**55.57±0.28**	**82.63±0.24**
Mahalanobis								
$k=1$	96.74±1.01	51.44±5.63	96.84±0.39	50.57±2.00	96.29±0.37	51.84±1.10	43.02±7.89	78.30±8.48
$k=2$	97.14±0.56	51.22±5.08	97.00±0.28	**50.83±0.39**	96.43±0.44	53.10±1.16	44.04±7.50	77.34±8.22
$k=3$	**97.44±0.18**	49.69±2.56	**97.03±0.06**	51.37±0.42	96.21±0.25	**54.42±0.46**	46.74±3.58	74.65±4.21
$k=4$	97.46±0.26	**51.52±0.86**	97.24±0.19	51.04±0.96	**96.58±0.21**	53.78±0.84	**43.83±0.45**	**78.34±0.54**
RankFeat								
$k=1$	87.91±8.24	63.17±11.47	82.25±6.77	73.38±7.74	85.79±5.13	68.94±6.86	63.83±9.05	79.96±5.41
$k=2$	81.78±12.13	65.91±13.15	75.24±7.78	77.17±4.21	80.77±5.67	71.95±3.88	48.51±12.19	87.40±4.45
$k=3$	**81.49±3.89**	67.76±5.56	68.66±5.92	80.83±3.01	75.58±3.89	75.22±2.65	40.32±5.00	90.61±1.64
$k=4$	76.87±4.21	**71.93±3.41**	**64.03±5.12**	**82.46±2.24**	**72.72±3.74**	**76.68±2.05**	**35.14±3.36**	**92.16±0.89**

Table 21: The detection performance of ensembling k modes (**ResNet50** trained on **ImageNet-1K**) on each OoD data set *w.r.t* different types of OoD detectors. The results with the **lowest variances** are highlighted with bold fonts.

Ensemble	OoD data sets							
of k modes	iNaturalist		SUN		Places		Textures	
	FPR↓	AUROC↑	FPR↓	AUROC↑	FPR↓	AUROC↑	FPR↓	AUROC↑
MSP								
$k=1$	58.38±1.87	86.99±0.45	70.41±0.93	80.96±0.32	72.70±1.17	80.01±0.37	66.32±1.29	80.62±0.26
$k=2$	54.69±1.01	88.29±0.24	68.75±0.39	82.03±0.04	70.72±0.37	81.21±0.12	64.05±0.57	81.58±0.05
$k=3$	53.57±0.55	88.75±0.19	68.31±0.21	82.18±0.09	70.74±0.37	81.38±0.12	63.39±0.48	**81.99±0.02**
$k=4$	**53.42±0.49**	**88.94±0.11**	**68.48±0.15**	**82.34±0.01**	**70.47±0.35**	**81.52±0.06**	**63.35±0.78**	82.11±0.07
ODIN								
$k=1$	53.33±3.14	89.67±0.80	58.43±1.70	86.19±0.50	63.44±1.80	84.31±0.76	53.51±1.28	86.43±0.22
$k=2$	50.60±2.55	91.06±0.56	56.50±1.54	87.37±0.40	61.09±0.96	85.47±0.46	49.41±0.93	**88.30±0.06**
$k=3$	48.43±0.89	91.76±0.15	**55.75±0.35**	**87.62±0.11**	60.59±0.49	**85.78±0.16**	**47.49±0.22**	88.86±0.14
$k=4$	**48.37±0.28**	**91.93±0.09**	55.81±0.50	87.74±0.14	**60.62±0.46**	85.89±0.20	46.52±0.57	89.13±0.08
Energy								
$k=1$	55.30±3.42	89.05±0.95	56.13±1.72	86.46±0.53	62.17±1.65	84.15±0.66	51.36±1.42	86.78±0.27
$k=2$	51.33±1.78	90.85±0.46	53.75±1.14	87.64±0.22	59.90±1.54	85.44±0.48	46.00±1.18	88.83±0.11
$k=3$	49.58±1.60	91.52±0.28	52.72±1.04	88.05±0.20	58.84±1.19	85.93±0.33	44.27±0.51	**89.48±0.03**
$k=4$	**49.23±0.97**	**91.64±0.20**	**52.33±0.27**	**88.23±0.07**	**58.34±0.57**	**86.14±0.10**	**42.74±0.43**	89.81±0.08
GradNorm								
$k=1$	71.53±3.96	78.41±2.98	71.25±2.38	75.76±1.44	78.96±2.38	71.51±1.49	65.24±1.49	77.74±0.95
$k=2$	69.97±3.93	79.96±2.53	68.72±1.53	77.06±0.94	77.15±1.67	72.93±1.08	61.93±0.88	79.85±0.41
$k=3$	67.58±2.53	81.99±1.44	67.78±0.41	77.97±0.32	76.43±0.49	73.69±0.27	60.71±0.75	**81.05±0.19**
$k=4$	**67.22±1.64**	**82.33±0.93**	**66.65±0.22**	**78.44±0.26**	**75.37±0.14**	**74.33±0.23**	**59.59±0.41**	81.52±0.21
Mahalanobis								
$k=1$	91.04±2.12	62.39±4.22	85.12±1.90	69.27±2.03	83.89±1.77	71.57±1.30	53.45±8.17	67.15±6.61
$k=2$	88.68±2.96	**65.43±2.15**	**83.44±3.27**	72.48±4.09	**83.41±2.78**	73.45±2.57	44.60±8.88	75.07±5.99
$k=3$	83.25±6.50	72.39±3.72	82.77±5.00	76.03±4.03	83.83±3.40	74.50±2.54	**37.22±7.31**	**82.91±4.23**
$k=4$	**81.49±2.78**	72.42±2.48	82.59±4.45	**76.15±3.11**	84.14±3.55	**74.44±2.07**	39.01±7.63	81.81±5.44
RankFeat								
$k=1$	63.06±13.98	84.15±3.34	54.87±17.18	86.58±4.57	65.86±12.20	80.71±3.99	37.87±10.59	91.86±1.51
$k=2$	49.18±13.04	89.67±2.61	45.30±11.30	89.80±2.57	59.64±8.77	83.70±2.61	23.21±2.71	**95.04±0.10**
$k=3$	45.78±10.18	90.96±1.93	43.45±3.39	90.57±0.82	**58.07±2.18**	84.49±0.69	**18.98±0.51**	95.98±0.25
$k=4$	**40.92±5.41**	**91.82±0.99**	**38.68±3.01**	**91.51±0.52**	54.84±2.31	**85.38±0.49**	16.44±0.77	96.43±0.36

Table 22: The detection performance of ensembling k modes (**DenseNet121** trained on **ImageNet-1K**) on each OoD data set *w.r.t* different types of OoD detectors. The results with the **lowest variances** are highlighted with bold fonts.